Performance, Efficiency, and Emissions Characterization of Reciprocating Internal Combustion Engines Fueled with Hydrogen/Natural Gas Blends

Final Technical Report

October 1, 2004 – June 20, 2007

Principal Authors

Kirby S. Chapman, Ph.D., Kansas State University

Amar Patil, Research Associate, Kansas State University

March, 2008

DOE Award DE-FC26-04NT42234

Submitted by

Kansas State University

National Gas Machinery Laboratory

245 Levee Drive

Manhattan, KS 66502

Disclaimer

Abstract

Hydrogen is an attractive fuel source not only because it is abundant and renewable but also because it produces almost zero regulated emissions.

Internal combustion engines fueled by compressed natural gas (CNG) are operated throughout a variety of industries in a number of mobile and stationary applications. While CNG engines offer many advantages over conventional gasoline and diesel combustion engines, CNG engine performance can be substantially improved in the lean operating region. Lean operation has a number of benefits, the most notable of which is reduced emissions. However, the extremely low flame propagation velocities of CNG greatly restrict the lean operating limits of CNG engines. Hydrogen, however, has a high flame speed and a wide operating limit that extends into the lean region. The addition of hydrogen to a CNG engine makes it a viable and economical method to significantly extend the lean operating limit and thereby improve performance and reduce emissions.

Drawbacks of hydrogen as a fuel source, however, include lower power density due to a lower heating value per unit volume as compared to CNG, and susceptibility to pre-ignition and engine knock due to wide flammability limits and low minimum ignition energy. Combining hydrogen with CNG, however, overcomes the drawbacks inherent in each fuel type.

Objectives of the current study were to evaluate the feasibility of using blends of hydrogen and natural gas as a fuel for conventional natural gas engines. The experiment and data analysis included evaluation of engine performance, efficiency, and emissions along with detailed in-cylinder measurements of key physical parameters. This provided a detailed knowledge base of the impact of using hydrogen/natural gas blends. A four-stroke, 4.2 L, V-6 naturally aspirated natural gas engine coupled to an eddy current dynamometer was used to measure the impact of hydrogen/natural gas blends on performance, thermodynamic efficiency and exhaust gas emissions in a reciprocating four stroke cycle engine. The test matrix varied engine load and air-to-fuel ratio at throttle openings of 50% and 100% at equivalence ratios of 1.00 and 0.90 for hydrogen percentages of 10%, 20% and 30% by volume. In addition, tests were performed at 100% throttle opening, with an equivalence ratio of 0.98 and a hydrogen blend of 20% to further investigate CO emission variations.

Data analysis indicated that the use of hydrogen/natural gas fuel blend penalizes the engine operation with a 1.5 to 2.0% decrease in torque, but provided up to a 36% reduction in CO, a 30% reduction in NO_X, and a 5% increase in brake thermal efficiency. These results concur with previous results published in the open literature. Further reduction in emissions can be obtained by retarding the ignition timing.

Table of Contents

Executive Summary

Hydrogen is an attractive fuel source not only because it is abundant and renewable but also because it produces almost zero regulated emissions.

Internal combustion engines fueled by compressed natural gas (CNG) are operated throughout a variety of industries in a number of mobile and stationary applications. While CNG engines offer many advantages over conventional gasoline and diesel combustion engines, CNG engine performance can be substantially improved in the lean operating region. Lean operation has a number of benefits, the most notable of which is reduced emissions. However, the extremely low flame propagation velocities of CNG greatly restrict the lean operating limits of CNG engines. Hydrogen, however, has a high flame speed and a wide operating limit that extends into the lean region. The addition of hydrogen to a CNG engine makes it a viable and economical method to significantly extend the lean operating limit and thereby improve performance and reduce emissions.

Drawbacks of hydrogen as a fuel source, however, include lower power density due to a lower heating value per unit volume as compared to CNG, and susceptibility to pre-ignition and engine knock due to wide flammability limits and low minimum ignition energy. Combining hydrogen with CNG, however, overcomes the drawbacks inherent in each fuel type.

Objectives of the current study were to evaluate the feasibility of using blends of hydrogen and natural gas as a fuel for conventional natural gas engines. The experiment and data analysis included evaluation of engine performance, efficiency, and emissions along with detailed in-cylinder measurements of key physical parameters. This provided a detailed knowledge base of the impact of using hydrogen/natural gas blends. A four-stroke, 4.2 L, V-6 naturally aspirated natural gas engine coupled to an eddy current dynamometer was used to measure the impact of hydrogen/natural gas blends on performance, thermodynamic efficiency and exhaust gas emissions in a reciprocating four stroke cycle engine. The test matrix varied engine load and air-to-fuel ratio at throttle openings of 50% and 100% at equivalence ratios of 1.00 and 0.90 for hydrogen percentages of 10%, 20% and 30% by volume. In addition, tests were performed at 100% throttle opening, with an equivalence ratio of 0.98 and a hydrogen blend of 20% to further investigate CO emission variations.

The key conclusion from these tests is the modest thermal efficiency gain of about 2% and significant emission reductions of between 18% and 45% when blending hydrogen with natural gas. The optimal fuel blend was found to be 20% hydrogen with 80% natural gas. Increasing the blend to 30% hydrogen did not, in most cases, achieve a significant reduction in emissions and reduced the power produced by the engine.

Results obtained can be summarized as follows for 20% hydrogen/natural gas blends when compared to the baseline data:

1. For an equivalence ratio of 0.9 and throttle opening of 50%
    a. Maximum reduction in torque is about 1.0%
    b. Maximum reduction in emissions of CO is about 36% and NO_X is about 15%

c. No significant change in BTE

2. For an equivalence ratio of 0.9 and throttle opening of 100%
   a. Maximum reduction in torque is 0.5%
   b. Maximum reduction in emissions of CO is about 25% and NO_X is about 18%
   c. Maximum increase in BTE is about 2.5%
3. For an equivalence ratio of 1.0 and throttle opening of 50%
   a. Maximum reduction in torque is 1%
   b. Maximum reduction in emissions of CO is about 45% and NO_X is about 31%
   c. No significant change in BTE
4. For an equivalence ratio of 1.0 and throttle opening of 100%
   a. Maximum reduction in torque is 2%
   b. Maximum reduction in emissions of CO is about 22% and NO_X is about 30%
   c. Maximum increase in BTE is about 3%

Further reduction in emissions can be obtained by retarding the ignition timing. As CO emissions were very sensitive to the equivalence ratio close to stoichiometric conditions, ignition timing was only retarded for an equivalence ratio of 0.9. A reduction in emissions in the range of 20 – 28% for CO and 60 – 65% for NO_X can be obtained by retarding the ignition timing. However, this will reduce the engine torque by about 5%.

Introduction

According to the Energy Information Administration, the most abundant human-caused greenhouse gas in the atmosphere is carbon dioxide (CO_2), which sits at the center of the recent climate change debate (Energy Information Administration, 2007). The primary cause of CO_2 is the combustion of fossil fuels with coal being the most carbon-intensive. Currently, much research has focused on the development of cleaner and more efficient uses of coal. Of particular interest are advances in coal gasification techniques that produce not only cleaner electric power, but also substantial amounts of hydrogen.

The opportunity to increase hydrogen production brings the need to develop technologies that facilitate the introduction of coal-derived hydrogen into the market. One such opportunity is the addition of hydrogen to compressed natural gas (CNG) engines to improve performance in the lean operating region. CNG-fueled engines are primarily used for short- and medium-distance over-the-road applications such as street sweepers, city buses, and trash trucks. These engines are increasingly popular alternatives because they produce less CO_2, particulate matter, and NO_X than gasoline or diesel fueled engines. Gasoline and diesel contain a higher carbon-to-hydrogen ratio than natural gas, which results in higher pollutant exhaust emissions. To date the high costs to process and transport natural gas via liquid natural gas tankers to fueling stations across the country has limited the widespread acceptance of CNG engines.

The addition of hydrogen to CNG engines extends operation further into the lean operating region, which reduces emissions and decreases fuel consumption. This occurs because hydrogen has a high flame speed and a wide operating limit that extends into the lean region. With natural gas alone as a fuel, the low flame propagation velocities are so low that operation in the lean region is severely restricted. These benefits make CNG-fueled engines a more attractive alternative to conventionally fueled engines and helps further develop a nation-wide hydrogen economy.

The main objective of this project is to study the impact of hydrogen/natural gas blends on the efficiency and exhaust gas emissions of a natural gas fueled engine. Basically this is an experimental work, where the effects of different hydrogen/natural gas blends at different engine loads and equivalence ratios are compared with baseline data obtained by using only natural gas as a fuel.

A literature review was first conducted to identify previous research that focused on using hydrogen/natural gas blends. Next, specifications of the engine, dynamometer, stand, fuel lines, and instrumentation were developed and then the test cell was assembled. After the tests were conducted, all collected data was reduced and analyzed and then compared to the baseline test of 100% natural gas. Data analysis includes the normalization of engine thermal efficiency and emissions, and subsequent correlation with equivalence ratio.

Conclusions include emissions and torque measurements for an optimized hydrogen percentage that are then compared with the data from the literature.

Literature Review

Oil accounts for approximately one-third of all the energy used in the world. The Energy Information Administration (Energy Information Administration, 2007) projects that world oil consumption of petroleum products will grow to 118 million barrels per day by 2030, as oil continues to be a major source of energy. Most of the studies estimate that oil production will peak by 2040 (GAO, 2007). Peak in production means half of the oil is removed and to remove the remaining half, more financial support is needed as compared with the cost of oil. According to the International Energy Agency, oil used for road transport grew from 500 million tonnes (5.51 million US short tons) oil equivalent (mtoe) in 1970 to nearly 900 mtoe (9.92 million US short tons) in 1990. Experts claim that about 21.3 millions of barrels per day or over one third of the world's oil production is in decline. The predicted declination rate is about 4%. Global demand for oil in 2003 had increased about 2% and in 2004 by about 3%. Oil prices ranged from $1 to $3 per million British thermal units (MMBtu) in 1990 and are projected at $6 per MMBtu in the near future (Skrebowski, 2004).

For example, consider the automobile industry, which consumes most of the oil. Japan, Canada and the U.S account for about 60% of the total car production. The total number of vehicles in 1950 was 50 million, which grew to 151 million in 1965, 369 million in 1985, and 479 million in 1996. It is estimated that the possible expansion in the automobile fleet will range up to 3 billion vehicles in 2050. Thus, the nations that depend on oil-producing countries will spend more money in buying oil (Campbell, 2002).

Standards of emissions for NO_X, non-methane hydrocarbons (NMHC) and particulate emissions are 5.364 g/kW-hr (4.0 g/bhp-hr), 1.743 b/kW-hr (1.3 g/bhp-hr), and 0.13 g/kW-hr (0.1 g/hp-hr), respectively (American Meteorological Society, 2000). The possible emissions standard to achieve by 2014 for heavy duty diesel engines as stated by Ryan, (2003) is to limit NO_X emissions to 0268 g/kW-hr (0.2 g/bhp-hr), NMHC to 0.188 g/kW-hr (0.14 g/bhp-hr), CO to 20.786 g/kW-hr (15.5 g/bhp-hr), and particulate emissions to 0.013 g/kW-hr (0.01 g/bhp-hr). The Clean Air Act Amendment also calls for a reduction in allowable sulfur content of diesel fuel from 500 ppm to 15 ppm.

Research to Improve Engine Performance and Reduce Emissions

The internal combustion engine (ICE) efficiency is limited by the compression ratio of the engine. In order to significantly increase the engine efficiency, an increase in the compression ratio is required. The increased compression ratio then leads to an increase in the peak in-cylinder temperature. Since NO_X formation is tightly coupled to the in-cylinder gas temperature, the increased in-cylinder temperature results in a corresponding increase in NO_X production. Edison and Taylor (1964) studied the impact of compression ratio on thermal efficiency. They concluded that, as compression ratio increases up to 300:1 (taking into consideration thermodynamic properties), the thermal efficiency for isooctane fuel at stoichiometric ratio is over 80%. Caris and Nelson (1959) studied the increase in thermal efficiency with the compression ratio on a V8 spark ignition engine, and found that, from a realistic standpoint, the thermal efficiency did not improve above a compression ratio of 17:1.

Increasing levels of greenhouse gases, a peak in oil production, higher world oil prices, and a limitation to increase the thermal efficiency of ICEs have created a need for an alternative fuel power system. As a result, researchers have focused attention on hydrogen. Its properties make it an excellent candidate for use as an engine fuel. Hydrogen can be produced by several methods, such as water electrolysis, natural gas, and coal gasification. The combustion of hydrogen in air produces only water and some oxides of nitrogen (by lean burning). Recent studies show that the desirable combustion properties of hydrogen make it the most likely candidate to eventually replace petroleum fuels (Azar et al., 2003). While most would argue that the establishment of a hydrogen-based economy is still far in the future, hydrogen augmentation to conventional fuels presents a viable mid-term solution for the transition to this new economy. The following discussion focuses on the impact of hydrogen/natural gas fuel blends on engine thermal efficiency and emissions. A sampling of this literature also describes the benefits and limitations of hydrogen dual-fuel engine operation, as well as the practical implications of this technology.

Aly and Siemer (1993) investigated the CO_2 minimizing effect of hydrogen addition to existing natural gas burning internal combustion engines for stationary power generation systems. The results obtained indicated an increase in thermal efficiency, as well as reduced emissions of CO_2, CO, NO_X, and unburned hydrocarbons.

Karim et al. (1996) investigated the properties of various methane-hydrogen fuel mixtures and the impact of these mixtures on overall engine performance, combustion, and emissions. While operating at relatively lean mixtures, researchers measured an increase in power output and work production efficiency, as well as a reduction in emissions. These improvements were determined to be due in part to the superior knock resistant qualities of methane maintained at lean mixtures, combined with the extremely rapid flame propagation rates of hydrogen. Van Blarigan and Keller (1998) investigated the feasibility of a hydrogen fueled internal combustion engine for both stationary and auxiliary power applications. They concluded that it is possible to construct a highly efficient power unit with equivalent zero emissions, fueled by a 30% hydrogen and 70% natural gas mixture.

Table 1 contains the properties of hydrogen and methane, which were compared as IC engine fuels by Verstraeten et al. (2004). They observed:

- The percent volume of the combustion chamber occupied by hydrogen is about 29.6% (refer to Appendix A) whereas methane occupies 9.6%, at stoichiometric conditions. As such, hydrogen limits the amount of the combustion chamber that can be filled with air, as compared to methane. For any given combustion chamber, there is less energy when using hydrogen (rich charge) than with methane. High pressure direct injection or liquid injection can overcome this drawback and can deliver more torque than methane.
- Hydrogen has a very wide flammability range in air (lower limit of 4% and upper limit of 75%) and therefore a hydrogen-fueled engine can operate with leaner mixtures. Lean mixtures provide the ability to capture load variations that result from perturbations (small change in physical system) due to the richness of the hydrogen-air mixture, which eliminates use of the throttle valve. The greatest benefit is improved engine efficiency due in part to the absence of flow losses and in part to combustion at a lower equivalence ratio.

Table 1: Properties of hydrogen and methane at normal temperature and pressure (Verstraeten et al., 2004)

Property	Hydrogen	Methane
Volumetric fraction of fuel in air at ϕ=1	0.296	0.09567
Limits of flammability in air, vol %	4 – 75	5.3 – 15
Laminar flame speed (m/s, ft/s)	1.9 (6.2)	0.38 (1.2)
Minimum spark ignition energy in air, (mJ)	0.02	0.29
Auto-ignition temperature (K)	858	813
Quenching gap in air,(m, ft)	0.00064 (0.00210)	0.00203 (0.0067)
Density (kg/m^3, lb/in^3)	0.08 0.0000029	0.717 0.0000258
Flame temperature in air (K)	2318	2148
Lower heating value (mJ/kg)	120	53
Higher heating value (MJ/kg)	141.7	52.68
Research octane number	-130	-120
Normal boiling point (K)	20.3	111.6

- The laminar flame velocity of hydrogen is about five times that of methane at stoichiometric conditions, as shown in Figure 1. This results in a more isochoric process (i.e., higher efficiency) and a more thermodynamically favorable combustion process (Heywood, 1988).

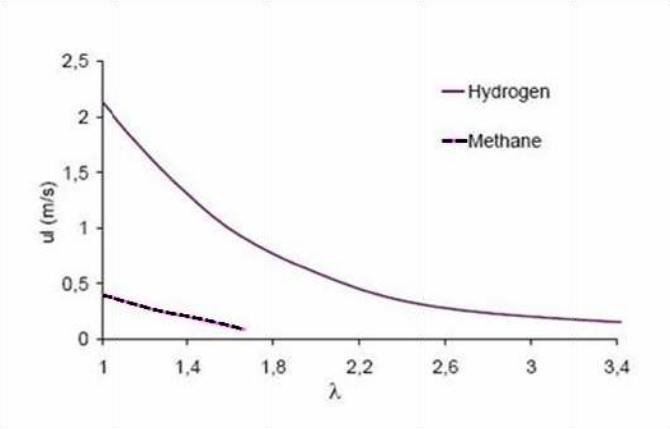

Figure 1: Variation of laminar velocity with air-to-fuel ratio ($\lambda = 1/\phi$) (Verstraeten et al., 2004)

- The necessary spark ignition energy of hydrogen at stoichiometric condition is 0.02 mJ (1.9^{-8} Btu)in air while methane requires 0.29 mJ (2.7^{-7} Btu) in air, as shown in Figure 2. This enables the ignition of very lean mixtures and ensures immediate ignition. Contact with hot spots or residual gas, however, can cause the mixture to spontaneously ignite and thus cause pre-ignition.

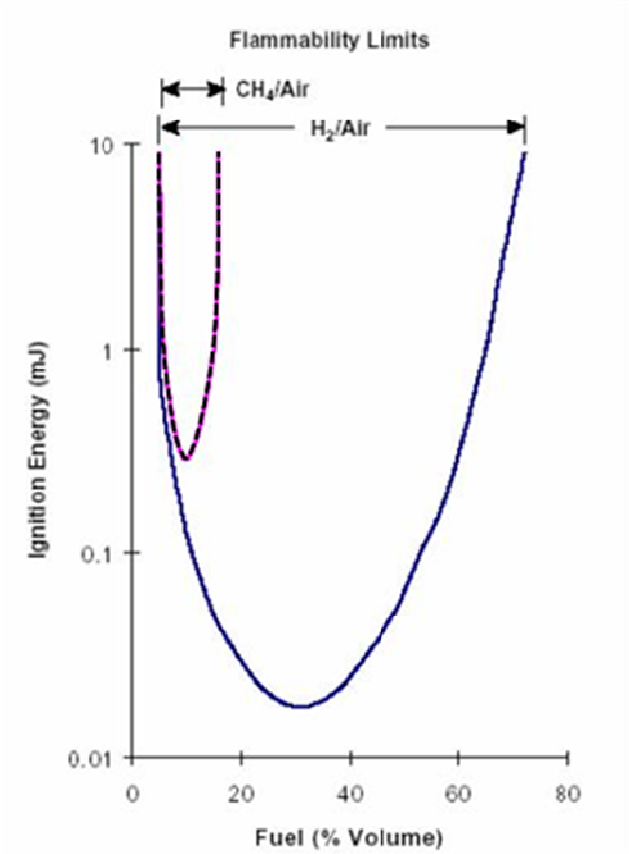

Figure 2: Ignition energy of hydrogen and methane (Alcock, 2001)

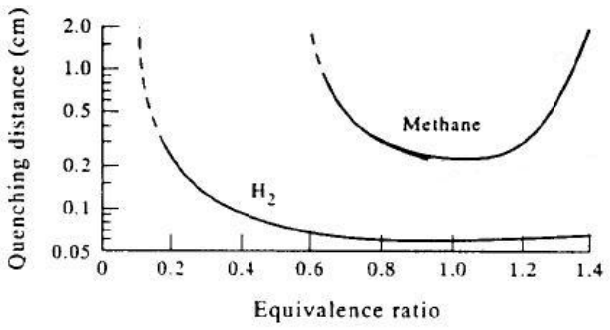

Figure 3: Quenching distance of hydrogen compared to methane (Das, 1990)

- Hydrogen has a higher auto-ignition temperature than methane. The auto ignition temperature limits the maximum compression ratio, and therefore, the maximum achievable engine efficiency. Hence, hydrogen can sustain a higher compression ratio and higher thermodynamic efficiency.
- Hydrogen has a quenching distance that is about three times smaller than methane, as shown in Figure 3. This implies that hydrogen can burn slowly in small and narrow crevices and thus cause pre-ignition.
- Hydrogen disperses in air at a much greater rate than methane. The density of hydrogen is 0.08 kg/m^3 (0.000003 lb/in^3) as compared to the density of methane at 0.717 kg/m^3 (0.000026 lb/in^3). This property makes it very easy to form a homogenous fuel-air mixture.

Verstraeten et al. (2004) concluded that pre-ignition was the main cause of limited torque in a hydrogen fueled engine. They also noted the advantages of using a throttle at very low loads and then fully opening the throttle at higher loads. NO_X concentration is a function of the trapped equivalence ratio (ϕ) and reaches a maximum at an equivalence ratio of 0.833. To limit NO_X concentration, Verstraeten et al. (2004) recommended operating with a trapped equivalence ratio of less than 0.58, but acknowledged that operating in this manner would limit power output from the engine.

Sierens and Verhelst (2001), conducted research on a General Motors V8 engine and concluded that sequential timed injection increased the resistance to pre-ignition. Cryogenic storage with direct injection in the combustion chamber using a pump was even better, but was not technically feasible for mass production. They observed that the power and torque output can be increased with a homogenous fuel mixture.

Bauer and Forest (1999) conducted a driving cycle analysis and collected performance and emissions data for varying mixtures of hydrogen and methane, equivalence ratios, speeds, and loads. In comparison with pure methane, adding hydrogen up to 60% by volume substantially reduced emissions of carbon compounds. Oxides of nitrogen emissions increased, however, as the percentage of hydrogen increased. Accompanying the general reduction in emissions was a corresponding reduction in brake power up to 8%, and a decrease in specific fuel consumption was observed as well.

Shrestha and Karmin (1999) investigated the impact of adding hydrogen to methane-fueled spark ignition internal combustion engines. The addition of hydrogen to methane increased performance, particularly during operation with lean mixtures at low equivalence ratios. Adding more than approximately 20% hydrogen by volume adversely affected power output and led to increased knock.

Shudo et al. (2000) investigated the effects on combustion and emissions of a methane-fueled direct injection stratified charge engine, premixed with hydrogen to form an overall lean air-to-fuel mixture. Hydrogen premixing increased thermal efficiency and decreased hydrocarbon exhaust emissions for lean operation. Hydrogen premixing did tend to increase NO_X emissions, but retarding the ignition decreased these emissions without adversely affecting thermal efficiency.

NO_X formation occurs when the in-cylinder gas temperature exceeds approximately 2000 K. Methods to lower NO_X emissions include direct injection of hydrogen, exhaust gas recirculation (EGR), variation of the injection starting point, and supercharging. Adding hydrogen to methane not only decreases emissions but also improves engine efficiency at lean fuel mixtures. (Nagalingam et al. (1983). Hydrogen is susceptible to pre-ignition because of its low octane number, while methane is not due to a relatively high octane number of approximately 120. The addition of hydrogen to methane results in the formation of a fuel mixture with more resistance to pre-ignition than hydrogen and other fuels. This is important since pre-ignition is a main concern with hydrogen blended fuels.

Direct-injection is another method to eliminate pre-ignition and back flash. In-cylinder injection utilizes a specially designed gas injector to inject hydrogen directly into the cylinder. This method improves the volumetric efficiency by eliminating hydrogen in the intake mixture, since only the original air-fuel mixture is present in the intake manifold. A study that utilized advanced numerical methods to model direct-injected hydrogen-fueled engines showed a reduction in NO_X emissions due to the broad flammability limits of hydrogen and fast combustion at extremely lean mixture conditions (Polasek et al, 2002). The study also concluded that most of the NO_X was formed in the post-flame region.

In lean-burn applications, NO_X emissions increase as the equivalence ratio increases from a lean mixture to near-stoichiometric mixture because of the increase in the in-cylinder temperature. An effective means to reduce NO_X during lean operation is to use EGR to circulate some of an engine's exhaust gas back to the engine cylinders where it serves as an inert gas and thereby lowers the peak in-cylinder temperature. While EGR is typically used on gasoline- and diesel-fueled engines, Heffel (2003) investigated the benefits of EGR on hydrogen-fueled engines over

a variety of engine speeds. He reported that EGR with the use of a three-way catalytic converter is an effective means to reduce NO_X emissions from hydrogen-fueled engines to less than 1 ppm.

Paul and James (2005) studied the effect of hydrogen/natural gas blends on emissions in lean-burn IC engines. They concluded that by increasing hydrogen concentration from 0 to 30% resulted in 55% reduction in CO emissions at part load and 40% at full load. NO_X emissions did not change much at mid-load operation, but at high load conditions and with a fixed equivalence ratio NO_X emissions increased drastically. Also, a 17% increase in efficiency was measured at mid-load for hydrogen addition up to 5%. Increasing hydrogen to 30% resulted in an additional 8% increase in efficiency. At full load, impacts of hydrogen addition on efficiency were statistically insignificant as compared to 100% natural gas.

Mechanisms of Pollutant Emission Formation

To fully understand methods to reduce pollutant emissions from IC engines, one must understand the formation of pollutants during the combustion process. This section explains the scientific basis of emission formation mechanisms and reviews relevant emissions reduction research.

Exhaust gases contain oxides of nitrogen (NO_X), carbon monoxide (CO), and unburned hydrocarbons. The combustion reaction of fuel is (Ferguson and Kirkpatrick, 2000):

$$C_\alpha H_\beta + \left(\alpha + \frac{\beta}{4}\right)\frac{1}{\phi}(O_2 + 3.76N_2) \rightarrow aCO_2 + bH_2O + cN_2 + dO_2 + eCO + fH_2 + gH + hO + jOH + kNO + lN + \ldots \quad (1)$$

where a, b, c, d, e, f, g, h, j, k, and l are the number of moles of the species per mole of fuel; and α and β are the number of carbon and hydrogen atoms in the fuel. The equivalence ratio, ϕ, is the ratio of the stoichiometric air-to-fuel to the actual air-to-fuel ratio.

Nitrogen Oxides

Nitric oxide (NO) and nitrogen dioxide (NO_2) are grouped together as NO_X emissions. Nitric oxide comprises the vast majority of the total oxides of nitrogen in the engine exhaust (Heywood, 1988).

The air-to-fuel ratio (AFR) plays a significant role in NO_X production. NO_X formation peaks on the fuel-lean side of stoichiometric when there is excess air for the quantity of fuel (Lefebvre, (1999). At this point, the fuel and nitrogen compete for the available oxygen. At high combustion temperatures, the atmospheric nitrogen and oxygen dissociates, which leads to the formation of NO_X. As an engine operates further into the lean region the combustion temperature decreases. This temperature reduction reduces the dissociation rate of N_2 and O_2, thereby decreasing the formation of NO_X. On the slightly rich side of stoichiometric, the NO_X formation is lower due to the lack of available oxygen.

Formation of Nitric Oxide

The principle reactions that govern the formation of NO from molecular nitrogen are given by the Zeldovich mechanism (Heywood, 1988):

$$O + N_2 \rightleftarrows NO + N \qquad E = -315 \text{ kJ/mol} \tag{2}$$

$$N + O_2 \rightleftharpoons NO + O \qquad E = 135 \text{ kJ/mol} \tag{3}$$

$$N + OH \rightleftharpoons NO + H \qquad E = 165 \text{ kJ/mol} \tag{4}$$

The forward reaction that is shown in equation (2) is an endothermic reaction. This reaction requires a temperature greater than 2,000 K to proceed due to the 315 kJ/mol of energy that is necessary to initiate the reaction. In the second reaction, equation (3), nitrogen atoms react exothermically with oxygen molecules to form nitric oxide and an oxygen atom. The third reaction, equation (4), is also exothermic and usually occurs in rich mixtures. The rate of formation for the first two reactions is given by (Heywood, 1988):

$$\frac{d[NO]}{dt} = k_{+1}[O][N_2] - k_{-1}[NO][N] + k_{+2}[N][O_2] - k_{-2}[NO][O] + k_{+3}[N][OH] - k_{-3}[NO][H] \tag{5}$$

$$\frac{d[N]}{dt} = k_{+1}[O][N_2] - k_{-1}[NO][N] + k_{+2}[N][O_2] - k_{-2}[NO][O] + k_{+3}[N][OH] - k_{-3}[NO][H] \tag{6}$$

The *k* terms are strong functions of temperature, as are the elemental equilibrium concentrations of O, N, and H. Therefore, the rate of formation of NO is extremely sensitive to flame temperature. As the burned gas region behind the flame front absorbs energy from the combusting mixture, the pressure and temperature rise significantly. In this high temperature region, NO is primarily formed whereas the flame front region produces an insignificant amount of NO. The flame front, however, provides the thermal energy required to dissociate the N_2 into N radicals and provides the reactions that lead to the NO producing chains. The main controlling factors in NO production are the amount of available oxygen and nitrogen radicals and the temperature of the mixture (Kenneth, 2005).

Formation of Nitrogen Dioxide

NO formed in the flame zone can be rapidly oxidized to NO_2 as shown by (Heywood, 1988):

$$NO + HO_2 \rightarrow NO_2 + OH \tag{7}$$

Conversion of NO_2 to NO only occurs when NO_2 formed in the flame is not quenched by mixing with cooler fluid as shown by (Heywood, 1988):

$$NO_2 + O \rightarrow NO + O_2 \tag{8}$$

Carbon Monoxide

Carbon monoxide is formed as (1) a result of incomplete combustion of fuel or (2) dissociation CO_2. CO emissions from internal combustion engines primarily depend on the equivalence ratio (Heywood, 1988). When the equivalence ratio is stoichiometric or moderately fuel-lean, then significant amounts of CO will be present because of dissociation of CO_2 (Lefebvre, 1999):

$$CO_2 \leftrightarrow \frac{1}{2}O_2 + CO \quad (9)$$

CO is readily formed in fuel-rich engines because of the lack of sufficient oxygen to complete the reaction to CO_2.

Hydrocarbons

Emission of hydrocarbons (HC) occurs because of incomplete combustion of the hydrocarbon fuel. Hydrocarbon emissions rise rapidly as the mixture becomes richer than stoichiometric. Lean-burn engines may also emit high levels of HC because of incomplete combustion (i.e., misfires) in just some of the operating cycles. Total hydrocarbon emission is a useful measure of combustion inefficiency. All hydrocarbons except methane react with NO_X to form photochemical smog. Reasons for unburned hydrocarbons include (Heywood, 1988):

- Flame quenching at the combustion walls
- Filling of crevices with unburned mixture
- Incomplete combustion in a fraction of the engine operating cycle
- Deposit build-up on the combustion chamber walls
- Leakage of charge through the exhaust valve

Summary

The literature suggests that hydrogen supplemented dual-fuel engine operation is a technically feasible means to reduce exhaust emissions from combustion engines and at the same time improve engine efficiency and performance. The excellent combustion properties of hydrogen make it a prime candidate for use as a fuel in dual-fueled engine, and presents a viable mid-term solution in the transition from conventional petroleum-based fossil fuels to hydrogen.

Previous research conducted with a 30% hydrogen/natural gas blend reduced emissions close to zero (Van Blarigan and Keller, 1998), while other research conducted at the same percent fuel blend demonstrated a reduction in CO emissions, but increased in NO_X emissions (Paul and James, 2005). A significant reduction in power was also reported for a 20% hydrogen/natural gas blend Shrestha and Karmin (1999). The major benefits of hydrogen-supplemented engine operation reported in the literature are reduced greenhouse gas emissions, reduced fuel consumption, and improved overall engine efficiencies. Despite its many benefits, there are a number of limitations associated with the practical implementation of this technology such as: pre-ignition, back flash and reduced engine power. The use of direct-injection, pre-combustion chambers, and exhaust gas recirculation to the fuel mixture are all promising methods to reduce the undesirable effects of hydrogen dual-fuel operation.

The literature indicated that the addition of hydrogen to conventional fuels combined with the above mentioned optimization techniques was the most successful means to reduce overall exhaust emissions and improve lean operation performance. An added benefit of hydrogen fuel engine operation is that the process requires minimal redesign of conventional engines in order to operate with hydrogen supplemented fuel mixtures. Advances in hydrogen reformation

techniques, engine technology, hydrogen storage and refueling issues will make this process a technically feasible and economically viable form of clean and renewable energy.

Experimental Set-up

A conventional natural gas engine was used to analyze the impacts of hydrogen/natural gas blends and to identify an optimal hydrogen/natural gas blend percentage. Figures 4 through 6 show the experimental set-up components that include the test engine, dynamometer, blending chamber (Figure5), engine control system (Figure 6), laminar air flow meter, fuel flow meter, and emission analyzer, each of which are discussed in the following sections.

Test Engine

A survey of commercially-available natural gas fueled engines determined that while there were many converted natural gas fueled engines on the market, only a few engines were solely designed as a natural gas fueled engine and were readily available. The natural gas fueled engine selected for this study was a Ford Power Products ESG-642. This is a six-cylinder naturally aspirated, four-stroke engine with spark ignition. Specifications for the engine are listed in Table 2. The engine was installed on the stand and aligned vertically with the dynamometer axis.

The engine included an engine performance module (EPM) to monitor and control engine performance via various sensors installed in the engine. These sensors included:

- Coolant temperature
- Intake air temperature
- Manifold air temperature
- Manifold absolute pressure
- Throttle position
- Foot pedal position
- Oxygen sensors
- Cylinder head temperature

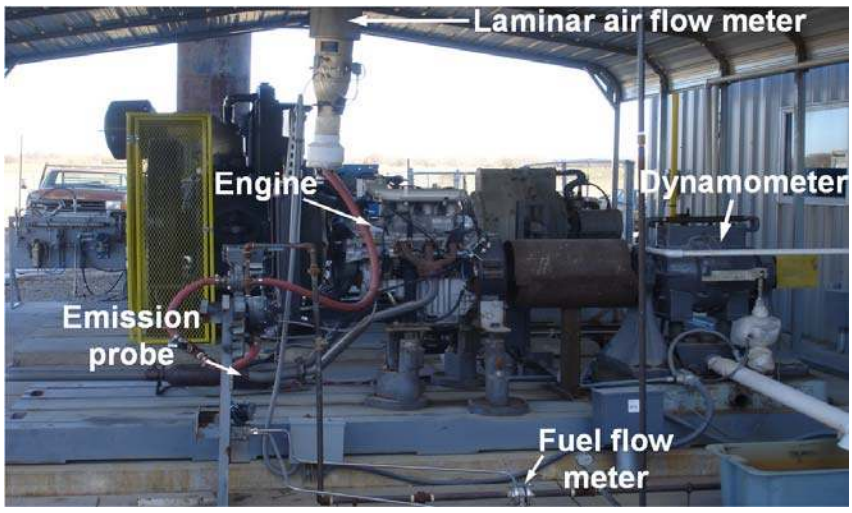

Figure 4: Experimental set-up

Figure 5: Blending chamber

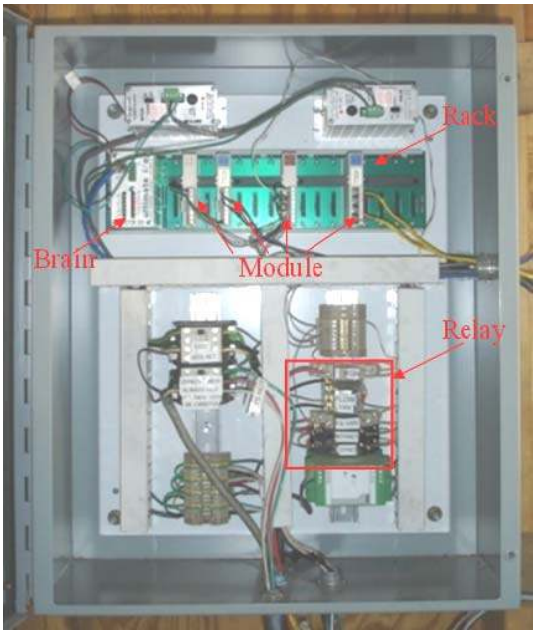

Figure 6: Instrumentation set-up for data collection

Table 2: Test engine specifications

Item	Specification
Engine type	V-6
Bore and stroke	96.8 mm x 95.0 mm (3.18 in x 3.74 in)
Displacement	4.2 litre (256 CID)
Compression Ratio	9.3:1
Oil Capacity	5.68 liters (6 quarts)
Net Weight	183 kg (403 lbs)
Base Engine Dimensions (H x L x W)	771.8 mm x 752.9 mm x 679.7 mm (30.3 in x 29.6 in x 26.7 in)
Continuous Gross Power	71 KW (97 hp) at 3,000 rpm
Continuous Gross Torque	256 Nm (189 ft-lbm) at 2,200 rpm
Maximum Speed	4,000 rpm
Capacity	4,195 cc (256 in^3)
Throttle Control	Electronic

In the event of a fault, the EPM codes can be displayed via a laptop computer. To understand how these sensors work together to provide critical operating information to the EPM, consider an example where the oxygen sensors and catalyst monitor sensors provide feedback to the EPM to control fuel flow. The EPM adjusts the fuel flow rate to maintain a prescribed equivalence ratio, which is necessary for proper catalyst operation. For this research, however, the EPM sensors were by-passed so that the engine could be operated in a variety of conditions.

Dynamometer

A Midwest 1014W wet-type eddy-current dynamometer was used to measure the brake power generated by the engine. The dynamometer applies brake torque to electromechanically absorb the power delivered by the engine. Water pumped through the dynamometer removes the heat generated by the applied torque. In addition to providing load, the dynamometer has a 60-tooth gear with a magnetic pick-up to measure engine rotational speed. The operating limits of the dynamometer are 250 hp and 6,000 rpm.

Blending Chamber

Figure 5 shows three compressed natural gas bottles that were used to premix hydrogen and natural gas in prescribed concentrations. Natural gas from a high pressure source was reduced to the required pressure and then mixed with bottled industrial grade hydrogen. The quantity of hydrogen mixed with natural gas was calculated by using gas equations of state and the partial pressures of each fuel.

Gases can be treated as ideal gases if the compressibility factor (Z) is near 1.0. The compressibility factor depends on the reduced pressure and temperature of the gas. The reduced pressure and temperature are functions of the actual and critical temperatures and pressures:

$$p_R = \frac{p}{p_{cr}} \qquad T_R = \frac{T}{T_{cr}} \tag{10}$$

The critical pressure for methane is 4,812 kPA (673 psia) and 1,345 kPA (188.1 psia) for hydrogen (Cengel and Boles, 2002). The compressibility factor is used to determine if a gas or a gas mixture can be considered ideal or real. The maximum pressure and temperature used in the experiments was 1,178 kPA (150 psig) and 540°R, respectively. Using Kay's rule, it was calculated that the compressibility factor is close to 1.0, which indicates that the mixture of natural gas and hydrogen gas can be modeled as an ideal gas with little uncertainty.

The percent volume by which hydrogen can be mixed with natural gas is calculated using Dalton's law of additive pressure and Amagat's law of additive volumes (Cengel and Boles, 2002). Dalton's law is given by:

$$p_{mix} = \sum_{i=1}^{n} p_i(T_{mix}, v_{mix}) \tag{11}$$

This explains that the pressure of a gas mixture equals the sum of the pressures that each gas exerts if it was alone at the stated temperature and volume. Amagat's law is given by:

$$v_{mix} = \sum_{i=1}^{n} v_i(T_{mix}, p_{mix}) \tag{12}$$

This explains that the gas mixture volume equals the sum of the volume that each gas occupies if it was alone at the stated temperature and pressure.

For ideal gases, p_i and v_i can be related to the mole fraction by:

$$\frac{p_i}{p_{mix}} = \frac{v_i}{v_{mix}} = \frac{n_i}{n_{mix}} \tag{13}$$

Equation (13) was used to create a prescribed natural gas/hydrogen blend.

The blending system, schematically shown in the lower portion of Figure 7, consists of supply lines from high pressure hydrogen and natural gas sources, valves for each, and the blending chamber. To operate the system, Valve A (lower right corner in Figure 7) was opened to fill the blending chamber to the prescribed pressure with natural gas. The prescribed natural gas pressure was determined by the desired percentage of hydrogen (e.g., 20 %) to be mixed with natural gas. Once the prescribed pressure was reached, Valve A was closed and Valve B was opened to admit hydrogen into the mixing chamber. Valve B was closed when the mixing chamber pressure reached 160 psig. The residence time for the hydrogen/natural gas blend was about 20 minutes.

This high pressure blend was reduced to a pressure of 377 kPA (38 psig) by using a pressure regulator and opening Valve C. Later, this blend flowed through an IMPCO Model E pressure regulator that reduced the gas pressure from 377 kPA (38 psig) to 3.8 – 6.3 cm (1.5 – 2.5 inches) of water at idle flow (approximately 750 rpm/no load). From the high pressure regulator, the fuel flowed into an electronic pressure regulator (EPR), which is part of the IMPCO Model E pressure regulator. The EPR reduced the fuel pressure depending on the feedback given by the EPM. The outlet pressure from the EPR varied from -2.5 – -12.7 cm (-1.0 – -5.0 inches) of water and depended on the engine speed and load. The air flow through the IMPCO 250 mixer caused the diaphragm to rise, which thereby controlled the amount of fuel entering the air stream. The amount of fuel entering the engine was altered by adjusting the EPR outlet pressure with the help of the EPM. This air fuel charge was then supplied to the engine via the throttle valve.

The following example demonstrates how to use equation (13) to calculate the pressures to achieve a specific percent of hydrogen.

Given:

Percentage of hydrogen by volume:	20%
Final pressure of the mixture:	1,247 kPA (174.4 psia)

Calculate the pressure of natural gas using equation (13):

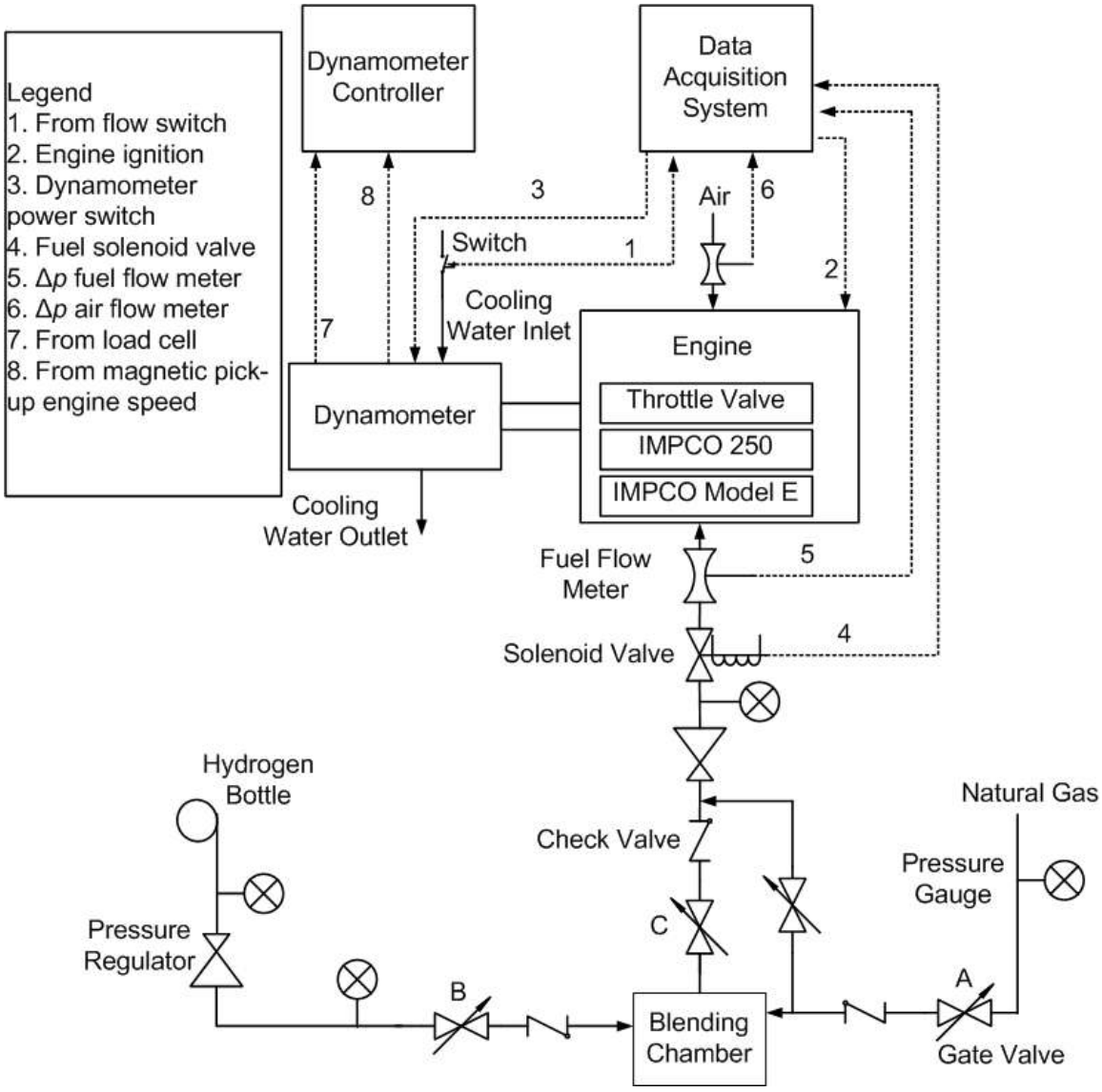

Figure 7: Process and instrumentation diagram

$$\frac{p_{CH_{4=}}}{1247} = y_{CH_4} = 1.0 - y_{H_2} = 0.8$$

$$p_{CH_4} = 1247 \times 0.8$$

$$p_{CH_4} = 997.5 \text{ kPA}$$

where 997.5 kPA is the equivalent of 139.5 psia.

Engine Control System

The engine control system houses all the controls and power for the engine as well as the data acquisition system. To collect data, an OPTO 22 SNAP Ethernet I/O system (Figure 6) was used

to digitize and transfer data into the computer. The SNAP Ethernet I/O system captured instantaneous values of the air and fuel flow rates. SNAP Ethernet I/O systems are based on open standards such as Ethernet and Internet Protocol and provided considerable data acquisition flexibility. The OPTO 22 Ethernet-based I/O unit consisted of a brain, I/O modules and mounting rack.

The SNAP-UP1-ADS Ultimate I/O brain served as the intelligent processor for distributed control. The I/O module provided the interface between signals received from field devices and the logic signals used in computers and controller. For this experiment, SNAP-AIMA-4, 4 channel, +/- 20 mA DC input modules, and IDC5R and ODC5R contractor modules were used. These modules received signals (4-20 mA) from pressure transmitters and converted the signals into numeric values that were interpreted by the computer. The I/O mounting rack, SNAP B16M, consisted of a board onto which the I/O modules and brain were installed, and provided connections between the I/O processor and the modules.

Figure 7 represents the general schematic of the process and instrumentation. The arrows on the lines show the direction of the gas/air flow and signals. The computer program managed the three following operations.

1. Safety of engine and dynamometer

The dynamometer used in this project required cooling water to remove heat released by the electromagnetic braking effect. To ensure an appropriate flow, a flow switch as shown in Figure 7 was installed in the cooling water flow path to the dynamometer. Also, Figure 8 shows the wiring layout of the flow switch connected to IDC5R module through a relay, which gave permission to start and run the engine based on the water flow rate.

2. Engine start up

As shown in Figure 7, a fuel solenoid valve was installed in the fuel line to close the fuel supply if a problem in the engine occurred. Once a positive command was given by the IDC5R module, the ODC5R module (refer to Figure 9) triggered the engine ignition, the dynamometer power switch, and the fuel solenoid valve to start the engine.

3. Data acquisition

Fuel and air flow rates were calculated by measuring the differential pressure across an orifice plate and with a laminar flow element, respectively. The principle of measuring instantaneous values of the air and fuel flow rates is similar. The differential pressure across an orifice plate/laminar flow element was transmitted to a pressure transmitter that converted the differential into a 4 to 20 mA signal. As shown in Figure 10, this mA signal was read and recorded by the OPTO 22 data acquisition system through an AIMA module that digitized the signal.

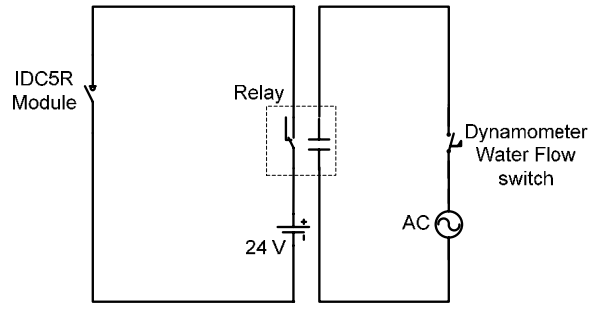

Figure 8: Wiring layout for dynamometer cooling water flow switch

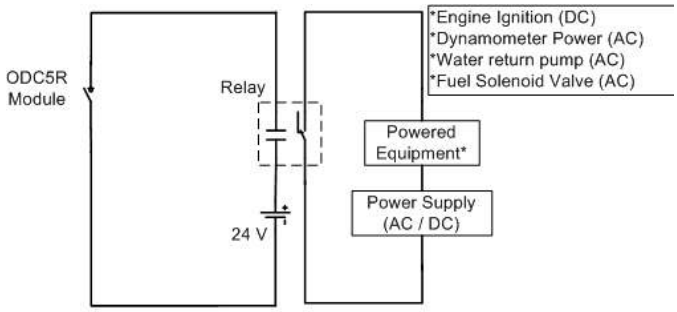

Figure 9: Wiring layout for engine start up

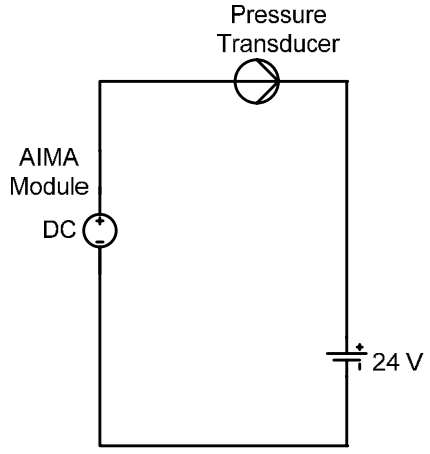

Figure 10: Wiring layout for data acquisition

Analog signals from the sensors were interfaced with the data acquisition system to digitize the analog signals. Table 3 provides the details about the types of sensors along with design parameters. Standard sensors that were included as an integral part of the engine control system are listed in Table 4.

Laminar Air Flow Meter

A Meriam laminar flow element (LFE), model 50MC2-4F, was used to measure the air flow rate through the engine. The LFE was calibrated with air at atmospheric conditions and referenced to 759.99 mm-HgA (29.92 in-HgA) and 21.1°C (70°F). A manufacturer supplied air flow rate calibration chart was used and appropriate corrections were made to account for variations in barometric pressure and ambient temperature.

Fuel Flow Meter

In order to test the engine at constant equivalence ratio, the LFE and a fuel flow meter were used to measure flow rates of air and fuel, respectively. The pressure differentials across these flow meters were transmitted by pressure transducers to the OPTO22 data acquisition system. These parameters were used to calculate efficiency, brake specific emissions and equivalence ratio.

Emission Analyzer

A Testo 350S Portable Compliance with Directive89/339/EEC emission analyzer was used to measure the exhaust gas emission concentrations. The measuring system included a control unit and a flue gas analyzer. The control unit was used to control, read, and program the flue gas analyzer. The flue gas analyzer housed sensors to measure CO, NO, NO_2 and O_2 concentrations. This analyzer had an integrated dilution system for extended

Table 3: Sensors installed on the engine

Description	Application	Range	Accuracy
Pressure Gauge	Natural Gas	105 - 1,893 kPA (0 - 250 psig)	±1.5% FS
	Hydrogen	105 – 17,892 kPA (0 - 2500 psig)	±1.5% FS
Pressure Regulator	Natural Gas	Up to 38.1 mm-WC (Up to 1.5 in-WC)	Unknown
	Hydrogen	Up to 334 kPA (Up to 32 psig)	±1.5% FS
Pressure Transmitter	Natural Gas and Hydrogen	4 – 20 mA	±0.1% FS
Pressure Transmitter	Air	0 – 152 mm-WC (0 - 6 in-WC)	±0.25% FS
Load Cell	Torque Measurement	0 – 227 kgf (0 - 500 lbf)	±0.1 mV
Thermocouple	Exhaust Gas Temperature	-98 – 1,371°C (-145 – 2,500°F)	±2°F
O_2 Sensor	Emission	0 – 25% vol.	±0.2% MV
CO Sensor	Emission	0 – 10,000 ppm	100 – 2,000 : ±5% mV
NO Sensor	Emission	0 – 3,000 ppm	2,001 – 3,000 : ±10% mV
NO_2 Sensor	Emission	0 – 500 ppm	±5% MV

Table 4: Standard OEM sensors

Measurement
Coolant temperature
Intake air temperature
Manifold air temperature
Manifold absolute pressure
Throttle position
Foot pedal position
Oxygen sensors
Cylinder head temperature

testing ranges and greater sensor protection. The Testo analyzer met EPA Conditional Test Method 034 Test Protocol (CTM-034) for monitoring O_2, NO, NO_2 and CO emissions. Figure 11 contains an illustration of the CTM-034 Test Protocol that was used. It consists of a pre-test verification, source test, and post-test verification. The pre-test and the post-test verifications use a known reference calibration gas, which allows for correction caused by drift in the electrochemical sensor. The source tests were individual tests taken during the engine

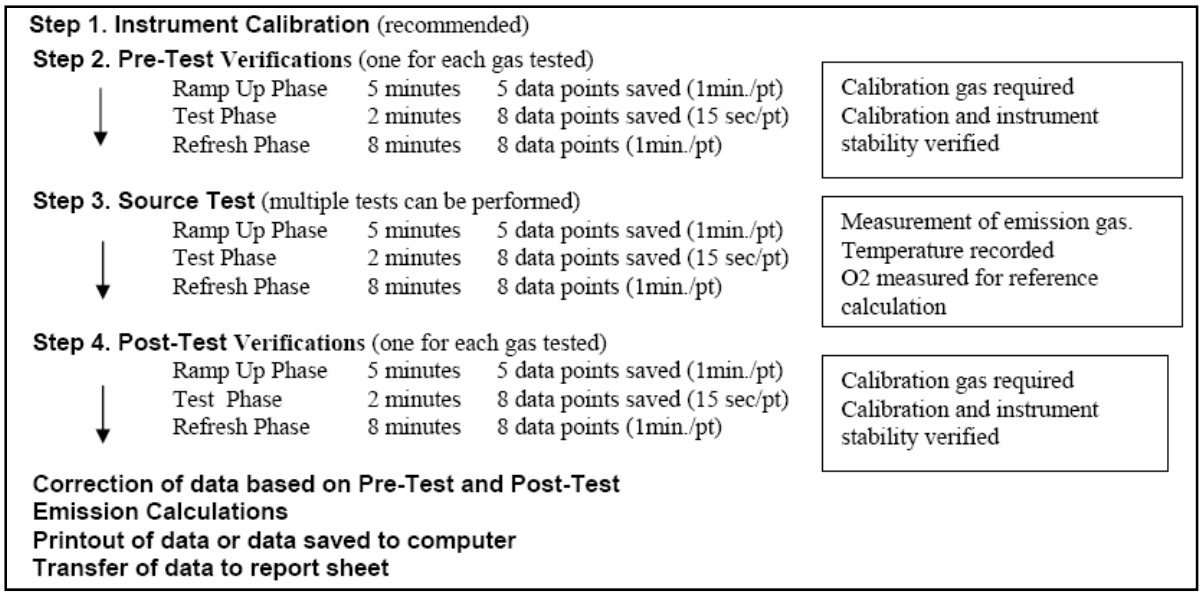

Figure 11: CTM-034 gas measurement test procedure (TSI Incorporated, 2004)

mapping. For the pre-, post-, and source tests the built-in CTM-034 Test Protocol used a ramp-up period of five minutes to stabilize the electrochemical sensors. Once stabilized, the test phase began and measurements were taken. After the test phase, the electrochemical sensors were purged with fresh air to allow them to recover.

According to Xavier (2000) uncertainty can be defined as "a parameter, associated with the result of a measurement that characterizes the dispersion of the values that could reasonably be attributed to the measured quantity, in other words, uncertainty is numerical information that complements a result of measurement, indicating the magnitude of the doubt about this result." The various sensors used in the experiment were subject to uncertainty in the form of random and systematic errors.

Random errors arise from unpredictable variations of influence quantities and cannot be completely eliminated. Increasing the number of observation can reduce this error. Systematic error arises from inaccuracies in instrumentation and calibration (Bevington and Robinson, 2002). Drift is an error that results when sensor calibration changes over time. For example, the electrochemical sensors in the emissions analyzer may have drifted over time from the original calibration. To alleviate this, the electrochemical sensors were calibrated frequently, typically before and after each use.

Throughout the experiment, a variety of instruments were used to measure engine performance and emissions. Each instrument had an associated accuracy, each of which appears in Table 3. The accuracy of each instrument was used to determine the uncertainty of each calculated value. First, the partial derivatives were calculated. With the partial derivative and accuracy known for each instrument, the uncertainty was calculated. Table 5 summarizes the uncertainty for calculated/measured parameters. Appendix B contains a complete example to calculate the uncertainty.

Table 5: Uncertainty for calculated parameters

Parameters	Uncertainty
Power	0.152 hp
BTE	0.000654
BSFC	3.113 g/kW-hr (2.321 g/bhp-hr)
ER	0.009594
Mass flow rate of air	5.086×10^{-4} kg/sec (0.00112 lbm/sec)
Mass flow rate of fuel	2.687×10^{-4} kg/sec (0.000592 lbm/sec)
CO	0.013 g/kW-hr (0.01 g/bhp-hr)
NO	1.613 g/kW-hr (1.203 g/bhp-hr)
NO_2	0.038 g/kW-hr (0.028 g/bhp-hr)

Engine Efficiency and Emissions Calculations

The objective of this research is to study the impact of the hydrogen/natural gas blends on the thermal efficiency and exhaust gas emissions of the selected natural gas fueled test engine. To accomplish this, the parameters that were measured included the pressure differentials across the orifice plate and laminar flow meter, ambient conditions, engine torque and speed, and exhaust gas emissions. The following section describes how these parameters were used to calculate engine efficiency and emissions.

Brake Horsepower

Brake horsepower of the engine was calculated in order to calculate engine efficiency and specific emissions rate. Specifically, torque and speed from the dynamometer controller were measured and recorded. Brake horsepower was calculated as:

$$\dot{W}_{act} = N\tau \tag{14}$$

The calculated brake horsepower was corrected to standard conditions to normalize data obtained at different ambient conditions. The correction factor is (Heywood 1988):

$$C_f = \frac{p_{std,d}}{p_m - p_{v,m}} \times \left(\frac{T_m}{T_{std}} \right) \tag{15}$$

The brake horsepower corrected to reference conditions was then calculated by:

$$\dot{W}_r = C_f \dot{W}_{i,m} - \dot{W}_{F,m} \tag{16}$$

For this particular engine, the friction power was estimated to be 5%.

Fuel Flow Rate

The fuel flow rate was measured with an orifice plate (Oripac 5300TM) fitted with a 4-20 mA differential pressure (Δp) transmitter (PX771A-1000WCDI). This parameter was needed in order to calculate the equivalence ratio, which is fully described below.

The fuel flow rate, $\dot{m}_f$ (kg/s) was calculated as per ISO 5167-2 (International Organization of Standards, 2003). The equation is given as:

$$\dot{m}_f \left[\frac{\text{kg}}{\text{sec}} \right] = \frac{e \times C \times A_{th}[\text{m}^2] \sqrt{2 \times \rho \left[\frac{\text{kg}}{\text{m}^3} \right] \times \Delta p \left[\frac{\text{N}}{\text{m}^2} \right]}}{\sqrt{1 - \beta^4}} \tag{17}$$

The gas expansibility e in equation (17) is defined as:

$$e \quad = 1 - \left(0.41 + 0.35 \times \beta^4\right) \times \frac{\Delta p[\mathrm{N/m^2}]}{k \times P_{in}[\mathrm{N/m^2}]} \tag{18}$$

Flow Rate of Air

The rate of air flow through the engine was measured with a Meriam laminar flow meter by:

$$\dot{V}_{a_{act}}[\mathrm{CFM}] = \left[B \times \Delta p[\mathrm{in}] + C_1 \times \Delta p^2[\mathrm{in}] \right] \left[\frac{\mu_{a_r}}{\mu_{a_{act}}} \right] \tag{19}$$

The viscosity of air at ambient conditions, as given by the manufacturer of the laminar flow meter, is:

$$\mu_{a_{act}} = \frac{14.58 \left(\frac{459.67 + T_{a_{amb}}[^\circ\mathrm{F}]}{1.8} \right)^{\frac{3}{2}}}{110.4 + \left(\frac{459.67 + T_{a_{amb}}[^\circ\mathrm{F}]}{1.8} \right)} \tag{20}$$

The standard volumetric flow of air was then calculated at 759.97 mm-HgA (29.92 in-HgA) and 21.1°C (70°F) is given by:

$$\dot{V}_{a_{std}} = \dot{V}_{a_{act}} \times \left[\frac{p_{act}}{p_r} \right] \times \left[\frac{T_r}{T_{act}} \right] \tag{21}$$

Brake Specific Fuel Consumption

The brake specific fuel consumption is a typical measure of the quantity of fuel required to produce a unit of power. In equation form, the brake specific fuel consumption combines equations (14) and (17):

$$\mathrm{BSFC} = \frac{\dot{m}_f}{\dot{W}_{act}} \tag{22}$$

Brake specific fuel consumption was used as a measure of engine efficiency.

Equivalence Ratio

The fuel and air flow rates were used to calculate the equivalence ratio. The equivalence ratio (ϕ) is the ratio of the stoichiometric air-to-fuel ratio to the actual air-to-fuel ratio. In equation form, the equivalence ratio is (Pulkrabek, 1997):

$$\phi = \frac{(AFR)_{stoich}}{(AFR)_{act}} \tag{23}$$

Volumetric Efficiency

The volumetric efficiency is a measure of the air flow losses in the engine air flow path. These losses occur due to the air filter, throttle plate, intake and exhaust valves, etc.

The volumetric efficiency is defined as (Pulkrabek, 1997):

$$\eta_v = \frac{2\dot{m}_a(\text{kg/sec})}{\rho_a(\text{kg}/\text{m}^3)V_d(\text{m}^3)N(1/\text{sec})} \tag{24}$$

where $\dot{m}_a$ is the actual air mass flow rate through the engine and V_d is the displacement volume of the cylinder.

For 100% volumetric efficiency, the temperature and pressure in the cylinder would be at atmospheric conditions. Typically, however, the trapped temperature is elevated due to heat transfer from the cylinder surfaces and the trapped pressure is below the barometric pressure due to pressure losses in the air flow path. Consequently, the density of the actual trapped mass is less than it would be at ambient conditions, which results in a volumetric efficiency less than 100%. The volumetric efficiency is a calculated ratio used to compare air flow path losses and restrictions in the engine system.

Mass Emission Rates

When measuring emissions, gas analyzers take readings in parts per million volume, or ppmv. However, for comparison purposes, a better method is to use mass based emissions units. For consistence in converting ppmv to mass based units the EPA uses Method 19. In the calculations in this study, the method used for converting ppmv emissions into mass based emissions is EPA Method 19 based on the O_2 F-Factor. Method 19 uses the mass flow rate of fuel and the measured oxygen content in the exhaust to determine the exhaust gas flow rate Q_d:

$$Q_d = F_{Btu}10^{-6}F_{O2}Q_f\left(\frac{20.9\%}{20.9\% - O_2\%_{measured}}\right) \tag{25}$$

Table 6: Density factors for exhaust gases

Component	Density Factor (d)	
NO_X	1.91×10^{-9}	g/cc-ppmv
	1.194×10^{-7}	lb_m/SCF-ppmv
CO	1.16×10^{-9}	g/cc-ppmv
	7.26×10^{-8}	lb_m/SCF-ppmv
Oxygen	6.66×10^{-10}	g/cc-ppmv
	4.155×10^{-8}	lb_m/SCF-ppmv
NO	1.25×10^{-9}	g/cc-ppmv
	7.792×10^{-8}	lb_m/SCF-ppmv

After calculating the Q_d factor, Table 6 can be used to find the density factors needed for different species of exhaust.

After calculating the exhaust gas volumetric flow rate and choosing the density which corresponds to the species being used. Equation (25) can be used to calculate the mass based emission rate of exhaust (Ely, 2004). By also dividing by the brake power, the size of the engine is removed from the exhaust and differently sized engines can be compared by this method as shown by:

$$E_{mass} = \frac{E_{ppmv} dQ_d}{\dot{W}_b} \tag{26}$$

Test Matrix and Procedures

Text Matrix

The test matrix consisted of two phases. The first phase established baseline engine parameters by measuring emissions and engine efficiency with natural gas as the sole fuel. In the second phase, the engine was tested with different concentrations of hydrogen and natural gas. The Phase 2 data were compared to the Phase 1.

The test matrix, shown in Table 7, was designed to minimize the variables and study the impacts of fuel type, ignition timing, engine load and speed. While the engine operating speed ranged from 800 to 3,000 rpm, the engine was tested in speed ranges associated with maximum torque since the test engine was primarily intended for stationary applications (as stated by engine manufacturer). Speeds of 1,800, 2,200 (maximum torque as per the manufacturer) and 2,600 rpm were selected for test.

The engine load was varied by changing the throttle valve position, for which 50% and 100% throttle opening were tested. These values were selected after initial testing with the throttle open at 25%, 50%, 75% and 100%. No significant difference in the engine power, torque and emissions data were observed at 75% and 100%. In addition, engine operation was not stable at 25% throttle opening. Hence, it was decided to conduct tests only for 50% and 100% throttle opening positions.

For the full test matrix, equivalence ratios of 0.90 and 1.00 were selected to determine the impact

Table 7: Test matrix

Throttle Open	Hydrogen	1,800 rpm	2,200 rpm	2,600 rpm
50%	0%	ϕ=0.9,1.0	ϕ=0.9,1.0	ϕ=0.9,1.0
	10%	ϕ=0.9,1.0	ϕ=0.9,1.0	ϕ=0.9,1.0
	20%	ϕ=0.9,1.0	ϕ=0.9,1.0	ϕ=0.9,1.0
	30%	ϕ=0.9,1.0	ϕ=0.9,1.0	ϕ=0.9,1.0
100%	0%	ϕ=0.9,1.0	ϕ=0.9,1.0	ϕ=0.9,1.0
	10%	ϕ=0.9,1.0	ϕ=0.9,1.0	ϕ=0.9,1.0
	20%	ϕ=0.9,0.98,1.0	ϕ=0.9,0.98,1.0	ϕ=0.9,0.98,1.0

of the addition of hydrogen at lean and stoichiometric conditions. At any given equivalence ratio the ignition timing was adjusted so that the engine developed maximum output torque. According to Heywood (1998), it is at this point that the in-cylinder peak pressure and peak combustion gas temperature were the highest, and produced the highest quantity of pollutants. The collected data were corrected to standard condition of 21.1°C (70°F) and 759.99 mm-HgA (29.92 in-HgA).

Fuel blends of 0%, 10%, 20% and 30% hydrogen in natural gas by volume were tested for the entire test matrix that is shown in Table 7. The only exception was that the engine was not tested at 100% throttle opening and 30% hydrogen concentration because the spark plugs continually failed, which caused the engine to misfire.

Finally, an additional data set was collected at an equivalence ratio of 0.98, 100% throttle opening, and 20% hydrogen fuel blend to quantify variations in CO emissions that were observed with small changes in the equivalence ratio.

Test Procedures

The procedure for testing the engine with only natural gas as a fuel was:

1. Start the engine with no load and run it at an idle speed of approximately 800 rpm.
2. Allow the engine to reach a steady state operating condition, which was when the cylinder head and the coolant discharge temperatures varied less than 1°F over a five minute period. These readings were monitored from the EPM.
3. Set the engine speed (1,800, 2,200, or 2,600 rpm) and throttle opening position (50 and 100%) to the desired value.
4. Set the fuel flow rate for the specified equivalence ratio and then adjust the ignition timing so that engine developed maximum output torque.
5. Collect the baseline data at the specified throttle opening position, equivalence ratio and spark timing.
6. Place the gas analyzer probe before the catalytic converter so as to nullify the effect of the catalytic converter on emissions.
7. Repeat all the tests at least two times to evaluate repeatability and to validate the data.

The general test procedure for hydrogen/natural gas blended fuel was similar to the baseline test with the following modifications:

1. Start the engine with no load and run at idle speed with pure natural gas.
2. Allow the engine to reach a steady state operating condition.
3. Gradually increase the engine speed and equivalence ratio to the target values and then adjust the ignition timing according to the maximum torque.
4. Switch the engine fuel from the pure natural gas to the hydrogen/natural gas blend and allow the engine to again reach a steady state operating condition.
5. Follow the baseline test procedure from step 3 to step 7.

6. Purge the storage fuel tanks several times with natural gas after each test to make sure the existing gas concentration would not influence the concentration of the newly filled mixture.

The final set of tests investigated the impact of ignition timing, and is explained in the analysis section that follows.

Data Analysis

The data analyses first were conducted at 100% load or wide open throttle (WOT) and then at partial load or 50% throttle open (TO). Data was analyzed for equivalence ratios of 0.9 and 1.0 for both cases and for 0.98 at WOT. Finally, data was analyzed for the case for retarded ignition timing.

Full Load Results

Torque

Figures 12 and 13 show the variation of torque with respect to engine speed at equivalence ratios of 0.9 and 1.0, respectively. As expected, higher engine torque (for baseline) was measured at an equivalence ratio of 1.0 (Figure 13), because of more fuel and maximum flame temperatures that occur slightly rich of stoichiometric (Heywood, 1988). This increased the internal energy (Heywood, 1988) and hence expansion work.

A reduction in engine torque was measured as hydrogen concentration increased. Taking into consideration uncertainty (Table 5) it can be concluded that for the equivalence ratio of 1.0 and 20% hydrogen concentration by volume, the maximum reduction in engine torque is approximately 2% when compared to the baseline data. The torque decreased only 0.5% for 0.9 equivalence ratio as compared with the baseline case. One plausible explanation is that the

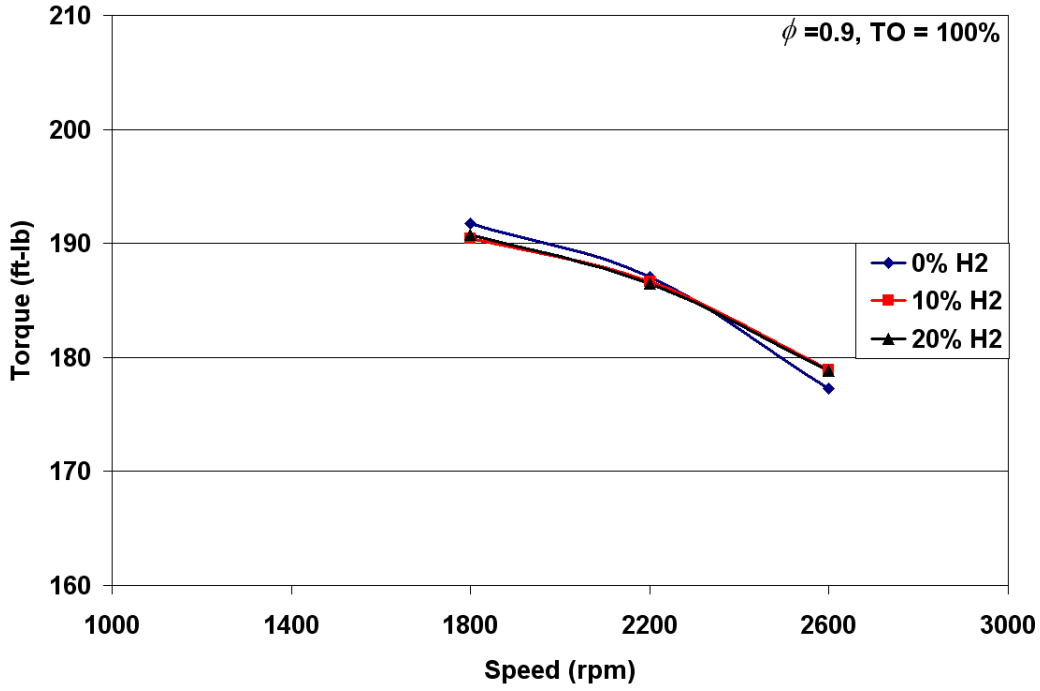

Figure 12: Variation of torque against speed for ϕ of 0.9 and TO of 100%

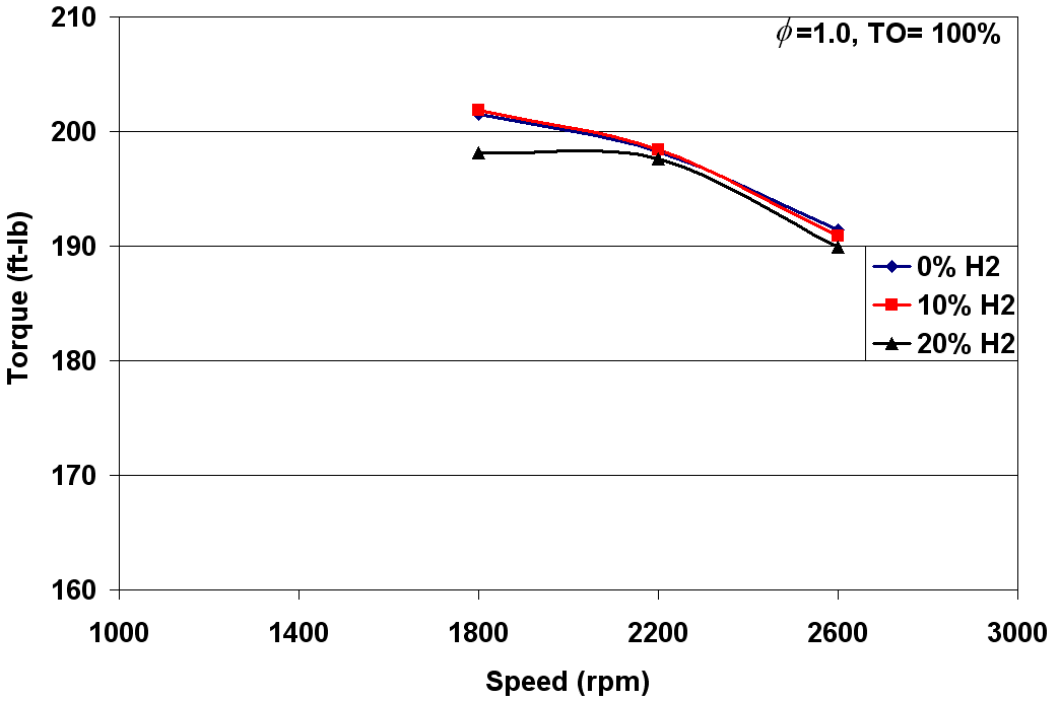

Figure 13: Variation of torque against speed for ϕ of 1.0 and TO of 100%

increased presence of hydrogen in natural gas fuels starts to adversely affect the power output due to lower volumetric heating value of the hydrogen/natural gas blends as shown in Figure 14.

A reduction in torque also was measured by Shrestha and Karim (1999) for hydrogen/natural gas blends more than 20%, but it was not specified as a percent reduction. According to Shrestha and Karim (1999) this might be because with lower equivalence ratios, the flame speed of the methane is usually quite low and the presence of the hydrogen with its superior burning rate characteristics enhances the overall burning rates of the mixture because of overall increase in laminar flame speed (Figure 1). As the equivalence ratio is increased toward stoichiometric, the increased presence of hydrogen makes less of a contribution.

CO Emissions

Figures 15 and 16 show the variation of CO emissions with respect to the engine speed at equivalence ratios of 0.9 and 1.0, respectively. CO emissions were less for the equivalence ratio of 0.9 as compared to 1.0. This might be due to the presence of excess air at an equivalence ratio of 0.9 which results in near complete combustion (Shrestha and Karim, 2005). Furthermore, according to Lefebvre (1999) if the equivalence ratio is equal to 1.0 or slightly fuel lean, then significant amounts of CO will be present due to the dissociation of CO_2 at high temperatures.

A maximum increase of about 60% in CO emissions, depending on speed, was measured for an equivalence ratio of 1.0 as compared to 0.9 at an engine speed of 2,600 rpm. In addition, a large fluctuation (sometime overshooting the limit of CO sensors) in CO emissions were measured as the equivalence ratio was moved from stoichiometric condition by a small amount (of about 0.01). Hence, an additional set of tests were conducted at an equivalence ratio (ER) of 0.98, which is close to stoichiometric. Data analysis for the ER of 0.98 appears later in this section.

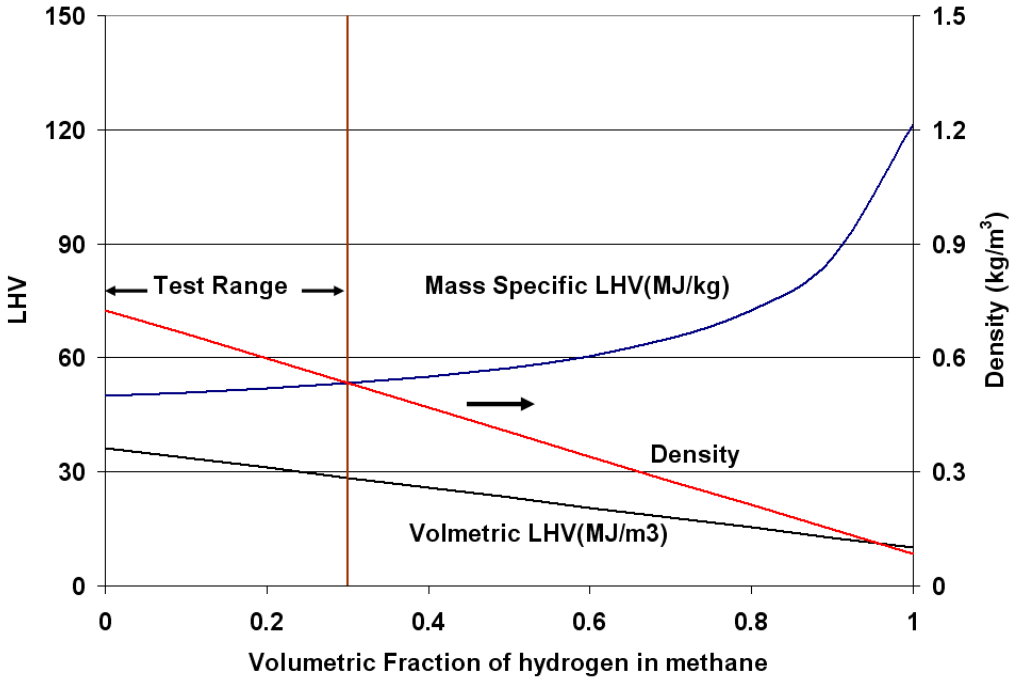

Figure 14: Variation of lower heating value and density of hydrogen/natural gas blends with volumetric fraction of hydrogen in methane

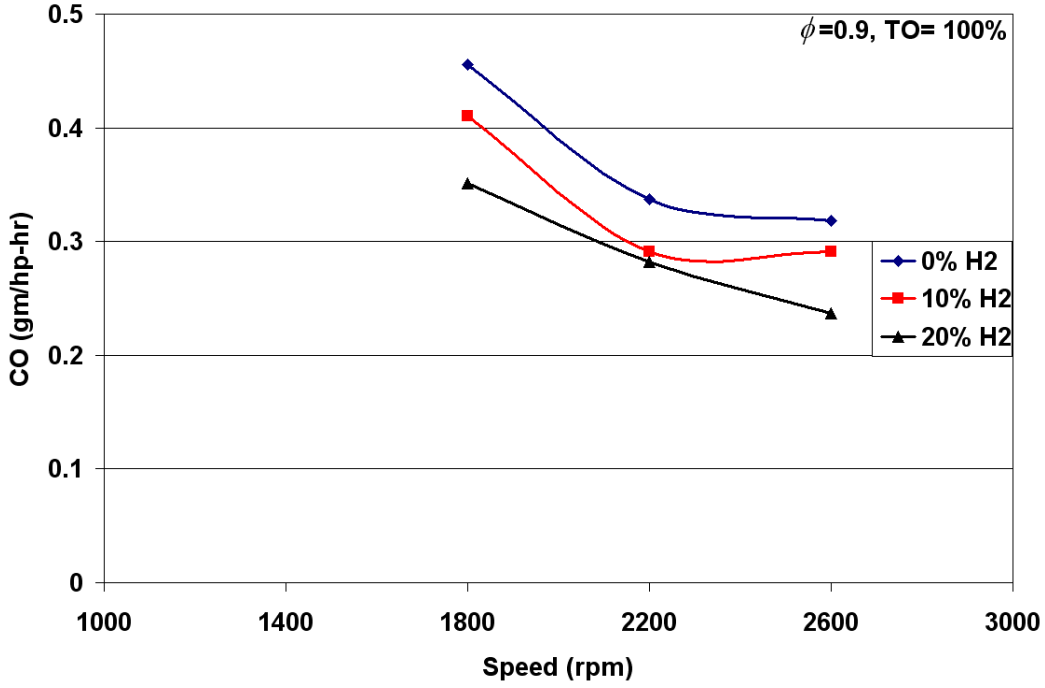

Figure 15: Variation of CO emissions against speed for ϕ of 0.9 and TO of 100%

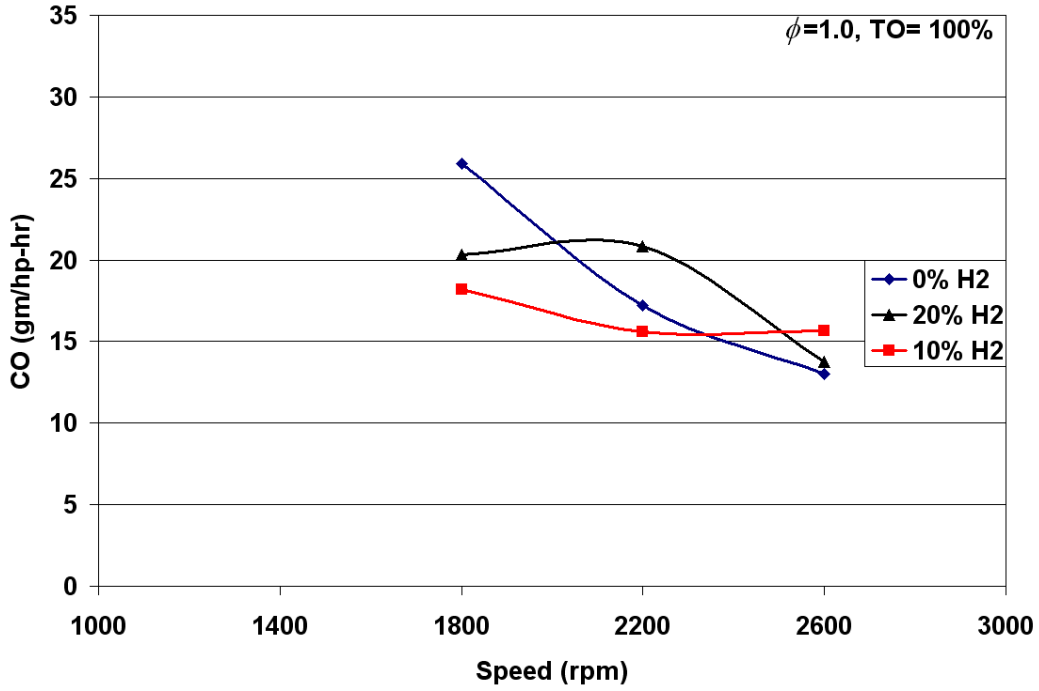

Figure 16: Variation of CO emissions against speed for ϕ of 1.0 and TO of 100%

It can be concluded using the uncertainty analysis (Table 5) from Figure 15 that CO emissions decreased as the percent hydrogen increased for an equivalence ratio of 0.9. A maximum reduction of about 25% in CO emissions was measured with 20% hydrogen/natural gas blend as compared with the baseline set, due to the absence of carbon atoms in hydrogen fuel that thereby lowered the hydrocarbon concentration in the fresh charge as the hydrogen percent increased, as shown in Figure 17. Similar results were measured by Van Blarigen and Keller (1998), Verstraeten et al. (2004), Bauer and Forest (1999), and Aly and Siemer (1993). At full load, Paul and James (2005) reported CO emission reductions of about 40% for a hydrogen/natural gas blend of 30%.

Conversely, an increase in CO emissions was measured for an equivalence ratio of 1.0, which does not agree with the literature. Similar results were obtained for an equivalence ratio of 0.98 as explained later in the section.

NO_X Emissions

Figures 18 and 19 show the variation of NO_X emissions with respect to the engine speeds at equivalence ratios of 0.9 and 1.0, respectively. It can be concluded from these plots that higher NO_X emissions are measured for an equivalence ratio of 0.9 as compared with 1.0. According to Lefebvre (1999), NO_X formation is found to peak on the fuel-lean side of stoichiometric because there is competition between limited fuel and nitrogen for the available oxygen. At this high combustion temperature the dissociation of atmospheric nitrogen and oxygen takes place that supports the formation of NO_X. Formation of NO_X in such a way is called thermal NO_X. The

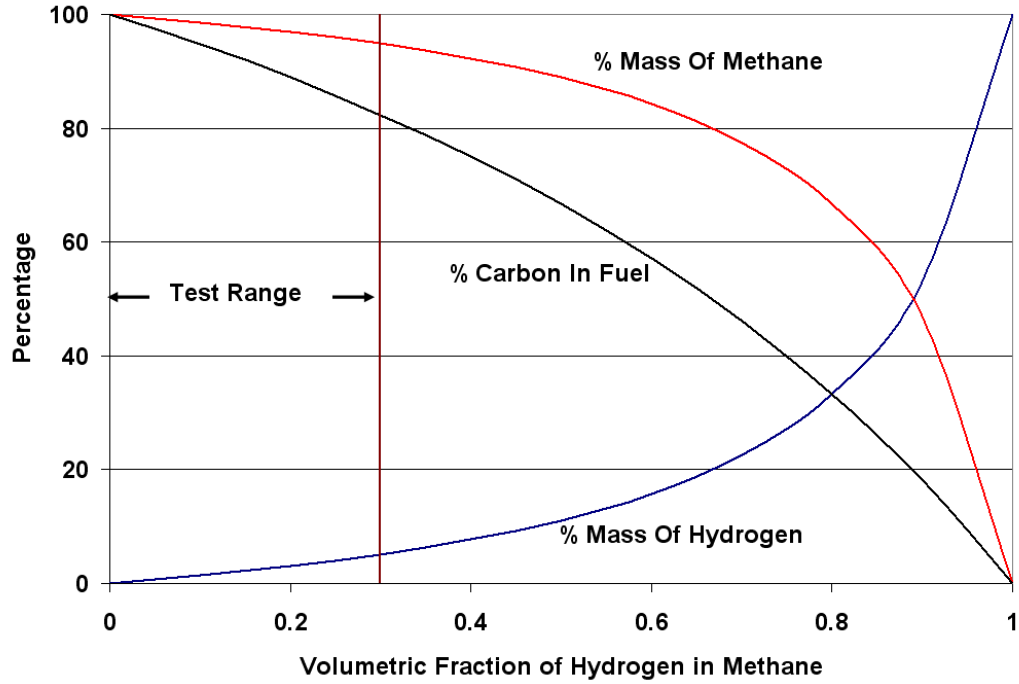

Figure 17: Variation of carbon percent in fuel with increase in volumetric fraction of hydrogen in methane

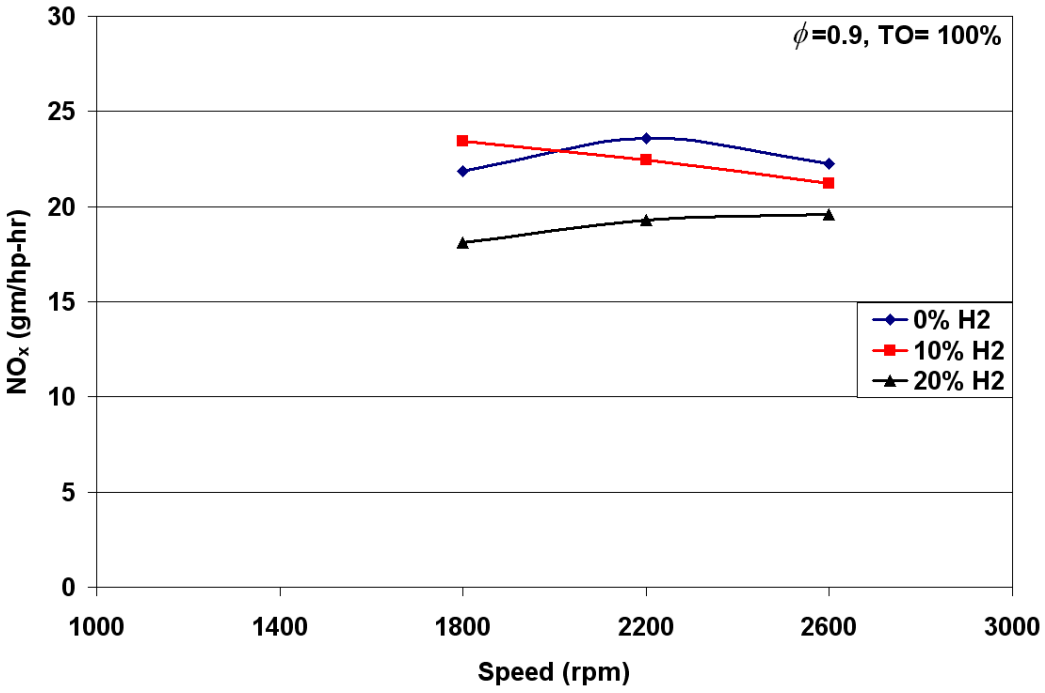

Figure 18: Variation of NO_X emissions against speed for ϕ of 0.9 and TO of 100%

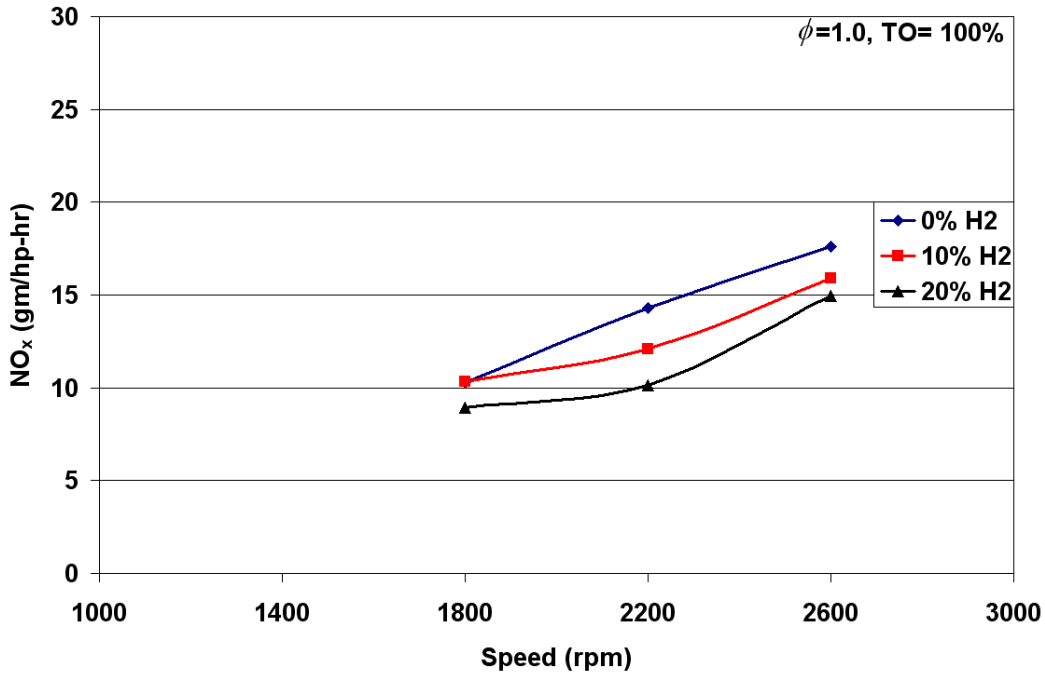

Figure 19: Variation of NO_X emissions against speed for ϕ of 1.0 and TO of 100%

formation rate of thermal NO_X almost exponentially increases as the temperature increases. Also, according to Das (1990) a heterogeneous charge can give rise to problems of incomplete combustion and high NO_X emissions. As the engine operates further into the leaner region, the combustion temperature decreases, and this effect dominates the kinetics of NO_X formation. In spite of the high combustion temperature on the slightly rich side of stoichiometric, the NO_X formation is lower due to the lack of available oxygen to supply O radicals as shown in equation (2).

After conducting an uncertainty analysis (Table 5), NO_X emissions were reduced 20% hydrogen/natural gas blends for both equivalence ratios as compared with baseline set. For a 0.90 equivalence ratio, the maximum NO_X reduction was 19%, and might be due to hydrogen mixing with air to form a homogenous mixture because of the higher diffusivity of hydrogen (Das, 1990). Furthermore, hydrogen has a higher flame propagation that reduces the combustion period during the expansion stroke (Das, 1996). For an equivalence ratio of 1.0 a maximum reduction in NO_X emissions is about 30%.

Verstraeten et al. (2004) measured the highest NO_X emissions at an equivalence ratio of 0.833. A reduction in NO_X was measured by Van Blarigan and Keller (1998) with 30% hydrogen/natural gas blends. Heffel (2003) reported a reduction in NO_X emissions to less than 1 ppm, but with the use of EGR and a three-way catalytic converter Gerbig et al. (2004) reduced NO_X emissions to almost zero. Paul and James (2005) reported increased in NO_X emissions at full load. Hence, the results of this study qualitatively compare to the data in the literature.

Brake Thermal Efficiency

Figures 20 and 21 show the variation of brake thermal efficiency (BTE) with respect to the engine speeds at equivalence ratios of 0.9 and 1.0, respectively. The BTE calculated at an equivalence ratio of 0.9 is about 5% greater than the BTE at an equivalence ratio of 1.0, which is consistent with Heywood (1988).

Figures 20 and 21 indicate that the BTE increases with the hydrogen percentage. After accounting for uncertainty, the maximum percentage increase in BTE is about 5% for an equivalence ratio of 0.9 and 2% for an equivalence ratio of 1.0 as compared to the baseline case. As stated by Andersson (2002), the improved efficiency depends on several factors. First, the addition of hydrogen increases the burn rate, which is beneficial for efficiency. Second, adding hydrogen improves the combustion efficiency to some degree. Third, the ratio of constant pressure and constant volume specific heats of the burned gas goes up with increased amount of hydrogen. For a 1.0 equivalence ratio, the increase in BTE for the 20% hydrogen/natural gas blend is less when compared to the 10% hydrogen/natural gas blends. Paul and James (2005) reported not much improvement in efficiency at full load, which agrees with these findings of a 2% increase after taking into consideration uncertainty.

Brake Specific Fuel Consumption

Figures 22 and 23 show the variation of brake specific fuel consumption (BSFC) with respect to engine speed at equivalence ratios of 0.9 and 1.0, respectively. The BSFC is the quantity of fuel required to produce a unit power output and can be related to BTE by:

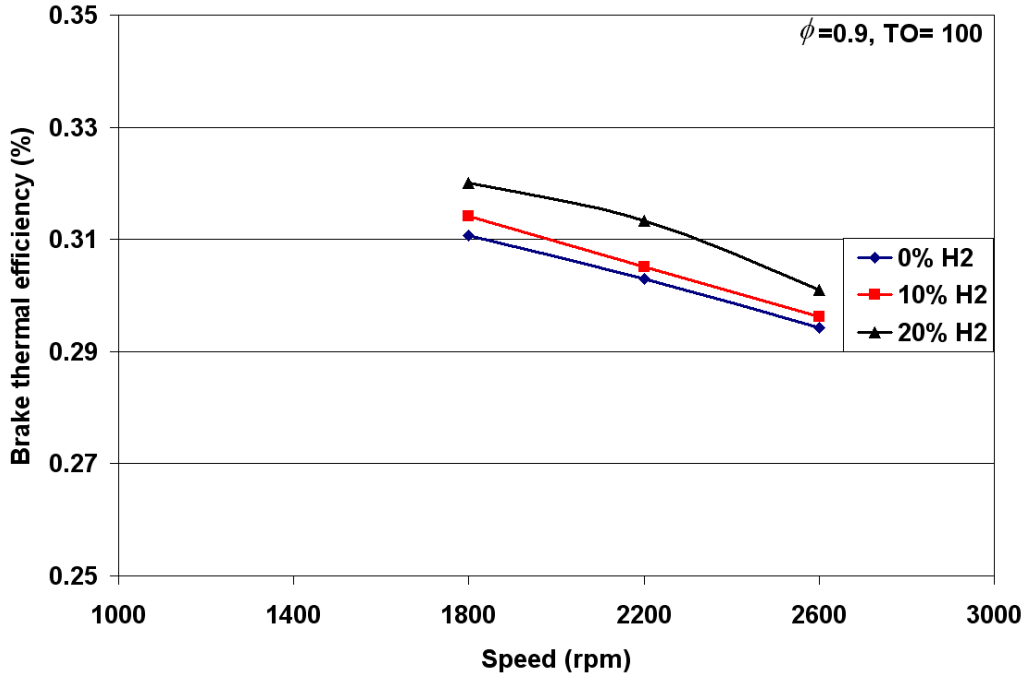

Figure 20: Variation of BTE against speed for ϕ of 0.9 and TO of 100%

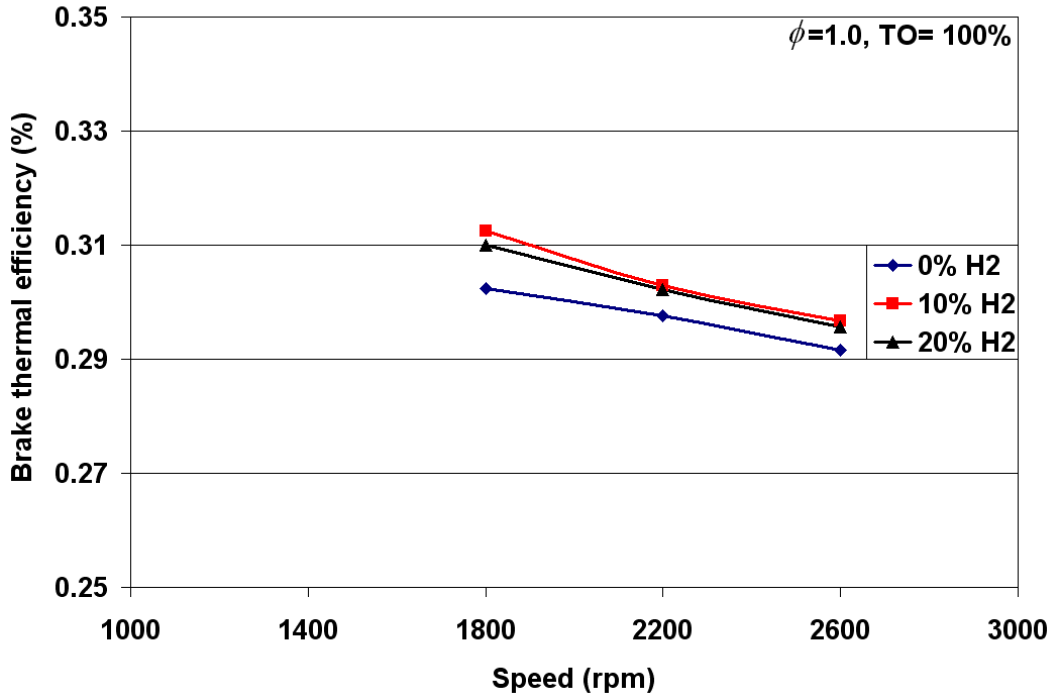

Figure 21: Variation of BTE against speed for ϕ of 1.0 and TO of 100%

$$\text{BSFC} = \frac{1}{\eta_b \times LHV} \tag{31}$$

The calculated values of BSFC for an equivalence ratio of 0.9 are lower than the BSFC at 1.0. This might be due to the decrease in BTE (as stated above) at stoichiometric conditions. Also, the combustion efficiency is high when using lean equivalence ratios, as measured with CO emissions. Combustion efficiency decreases for rich equivalence ratios by approximately $1/\phi$ as there is insufficient oxygen to complete combustion (Bauer, 1999).

After statistical analysis (Table 5), the maximum reduction in BSFC for a 0.90 equivalence ratio was 10% and 7% for a 1.0 equivalence ratio as compared with the baseline case. Bauer and Forest (1999) measured similar reductions in BSFC. As hydrogen percentage increases the BSFC decreases (refer to equation (31)) because of higher energy contents of the fuel associated with the addition of hydrogen (Figure 14). Also, as the engine speed increases the BSFC increases due to higher friction power associated with speeds.

Equivalence Ratio 0.98 and 100%Throttle Opening

Because of the rapid increase in CO at slightly lean operation, a set of experiments was conducted at an equivalence ratio of 0.98. From the above plots it could be concluded that a 20% hydrogen/natural gas blend reduces emissions without significantly affecting engine performance. Hence, only 20% hydrogen/natural gas blend was used to test the engine at an equivalence ratio of 0.98. Figures 24 through 28 show the variations of torque, CO emissions,

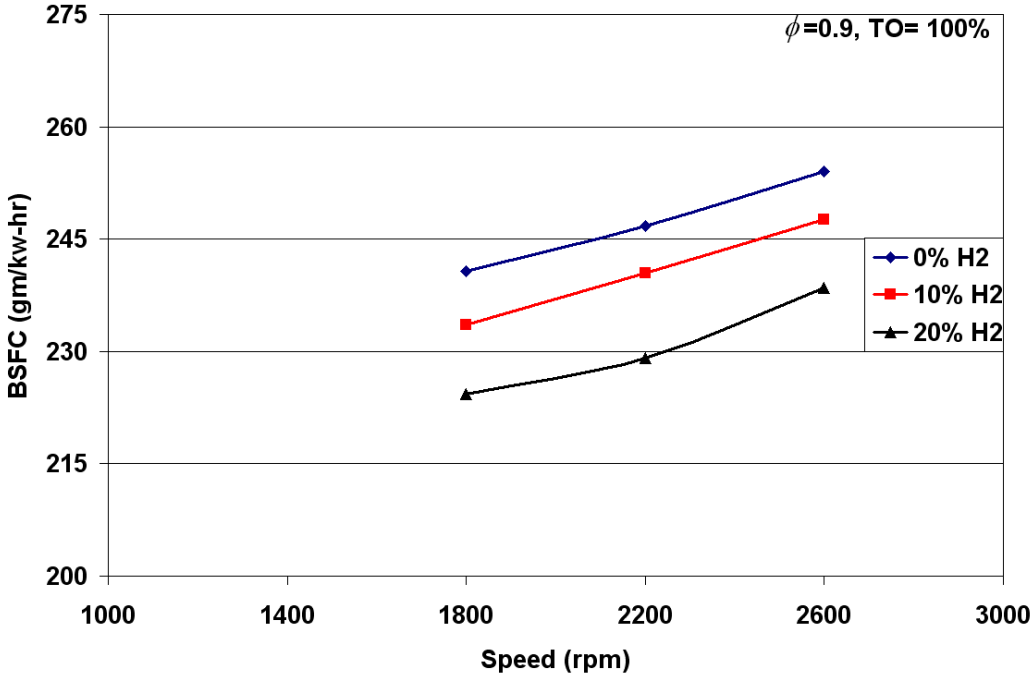

Figure 22: Variation of BSFC against speed for ϕ of 0.9 and TO of 100%

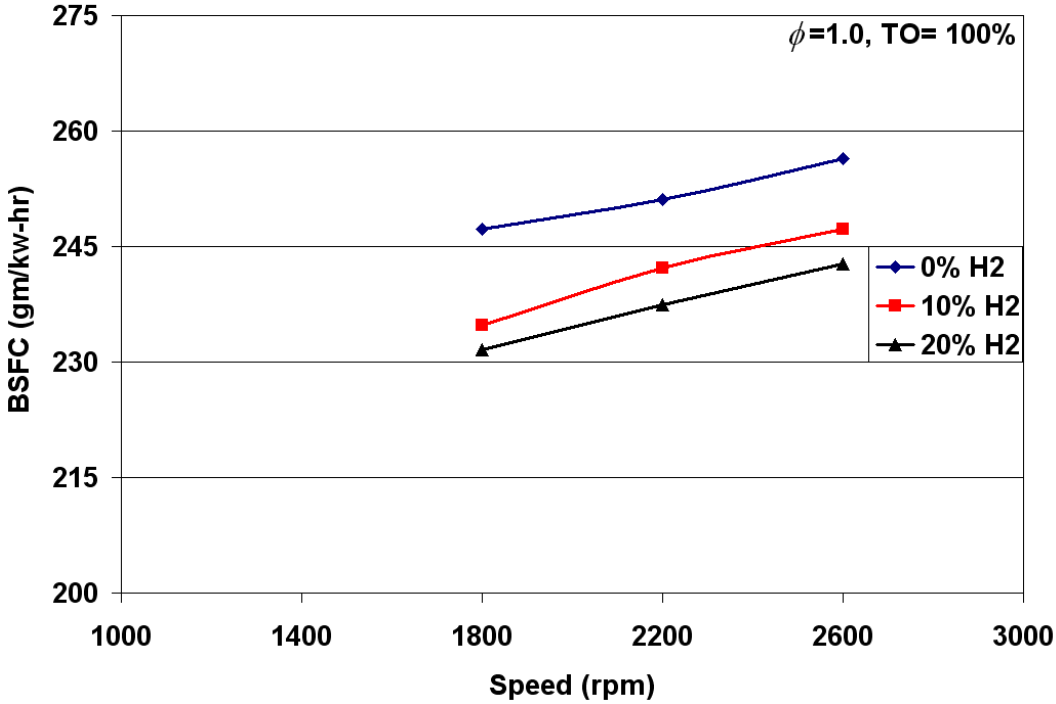

Figure 23: Variation of BSFC against speed for ϕ of 1.0 and TO of 100%

NO_X emissions, BTE and BSFC with respect to engine speed. These plots follow similar trends as reported above. Table 8 provides a summary of these plots with the maximum percentage reduction (+ indicates percentage increase) with reference to the baseline data.

As shown in Figure 25, CO emissions were higher than the baseline for a 0.98 equivalence ratio with 20% hydrogen. The dominant oxidation reaction for carbon monoxide in an engine is (Heywood, 1988):

$$CO + OH \leftrightarrow CO_2 + H \tag{32}$$

The oxidation of CO depends on the availability of the OH radicals and competes with the hydrocarbon concentration. As CO oxidation has a relatively higher activation energy, its oxidation is delayed until the original hydrocarbon and the intermediate hydrocarbon species have been consumed. OH concentration then rise to higher levels, which that thereby convert the CO to CO_2 (Kenneth, 2005).

The concentrations of CO and CO_2 for equation (32) can be related to the concentration of H and OH radicals as:

$$\frac{[CO]}{[CO_2]} = \frac{1}{K}\frac{[H]}{[OH]} \tag{33}$$

The term K is the equilibrium constant and [CO], [CO_2], [H], and [OH] are the respective concentrations of carbon monoxide, carbon dioxide, hydrogen and hydroxyl radicals.

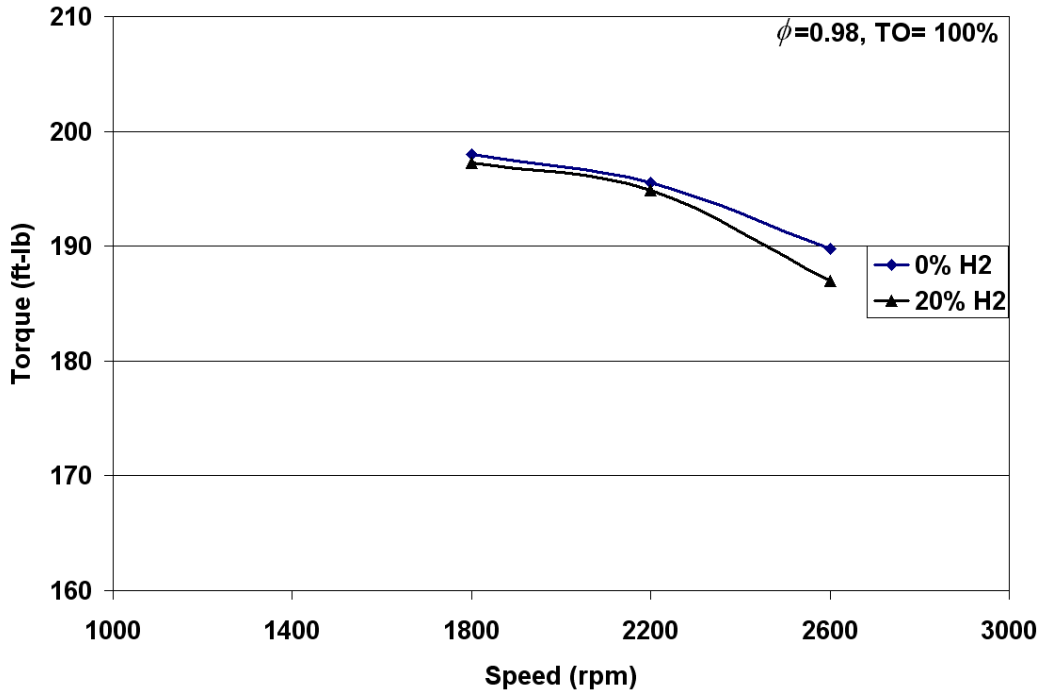

Figure 24: Variation of torque against speed for ϕ of 0.98 and TO of 100%

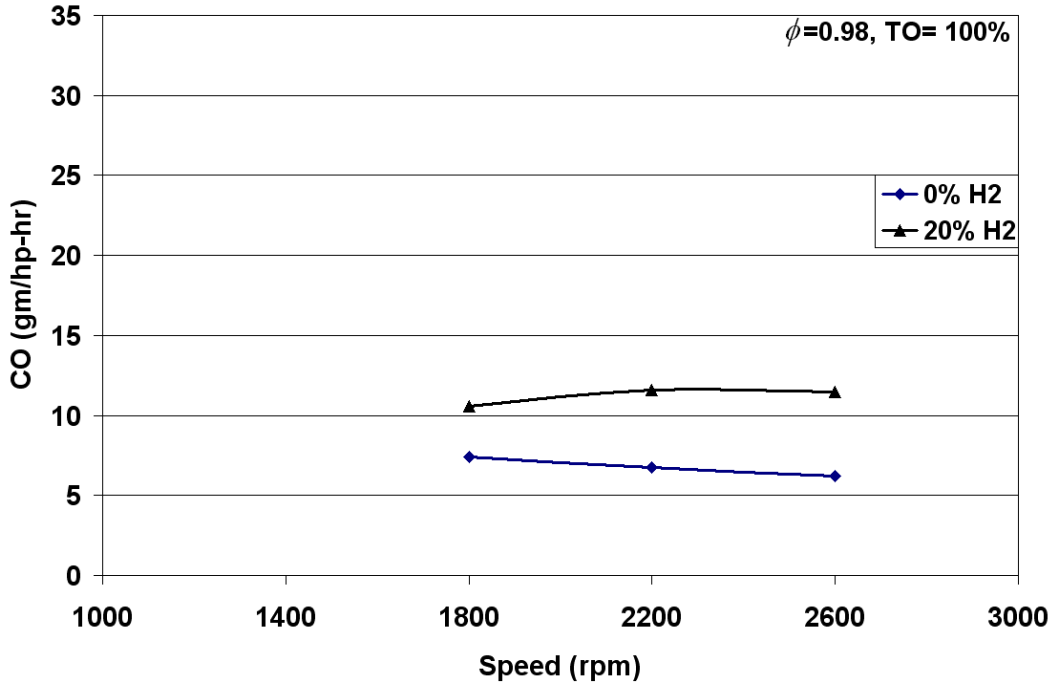

Figure 25: Variation of CO emissions against speed for ϕ of 0.98 and TO of 100%

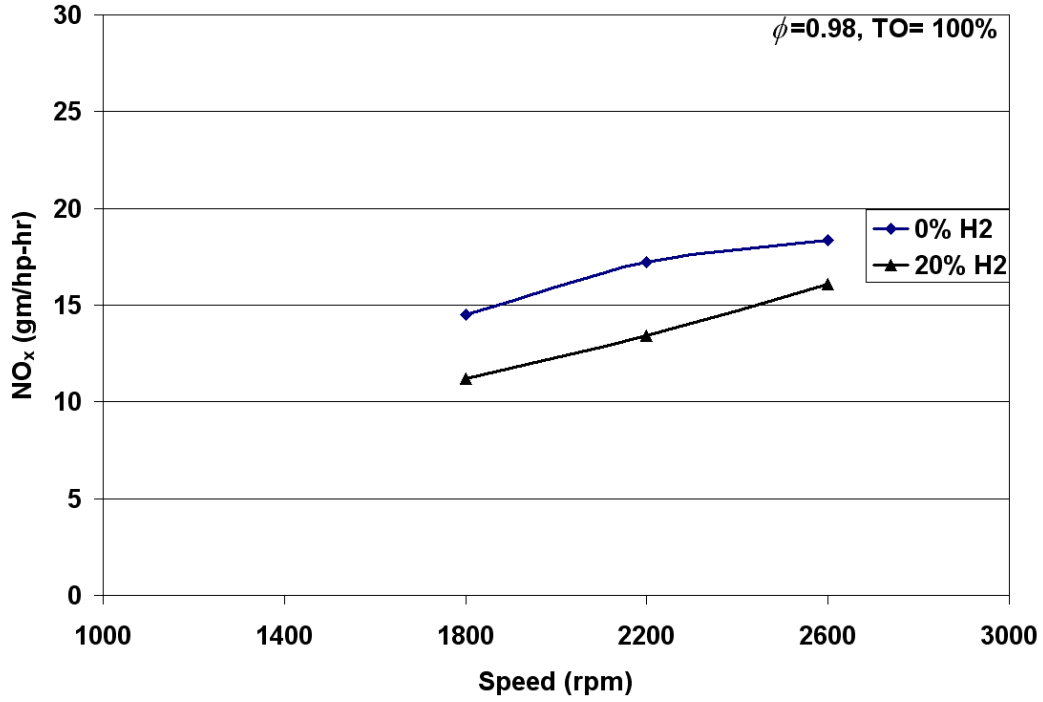

Figure 26: Variation of NO_X emissions against speed for ϕ of 0.98 and TO of 100%

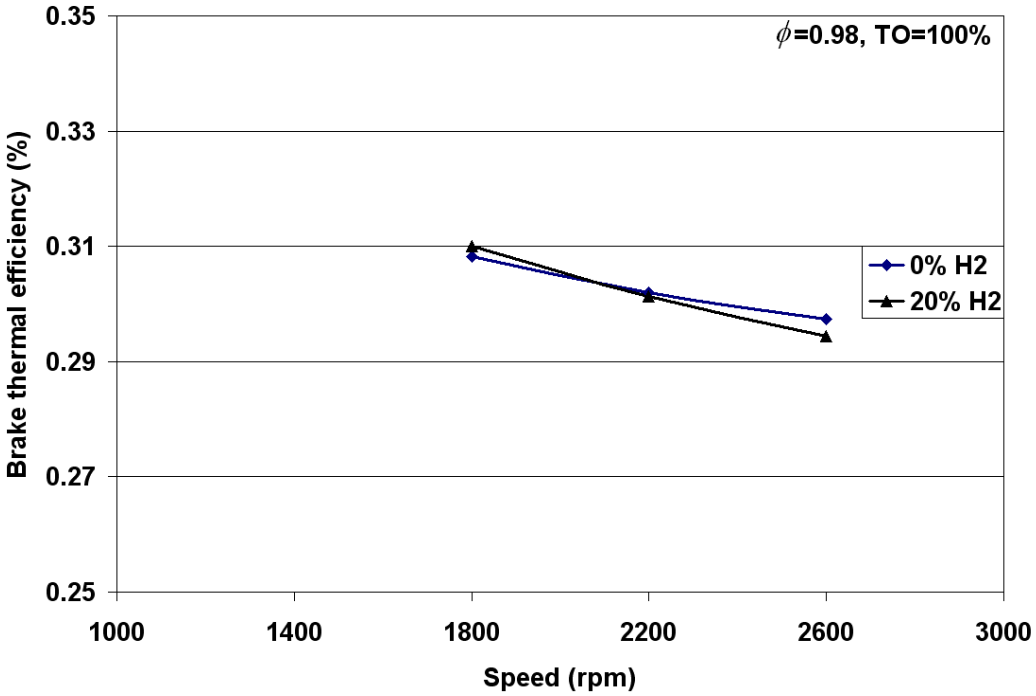

Figure 27: Variation of BTE against speed for ϕ of 0.98 and TO of 100%

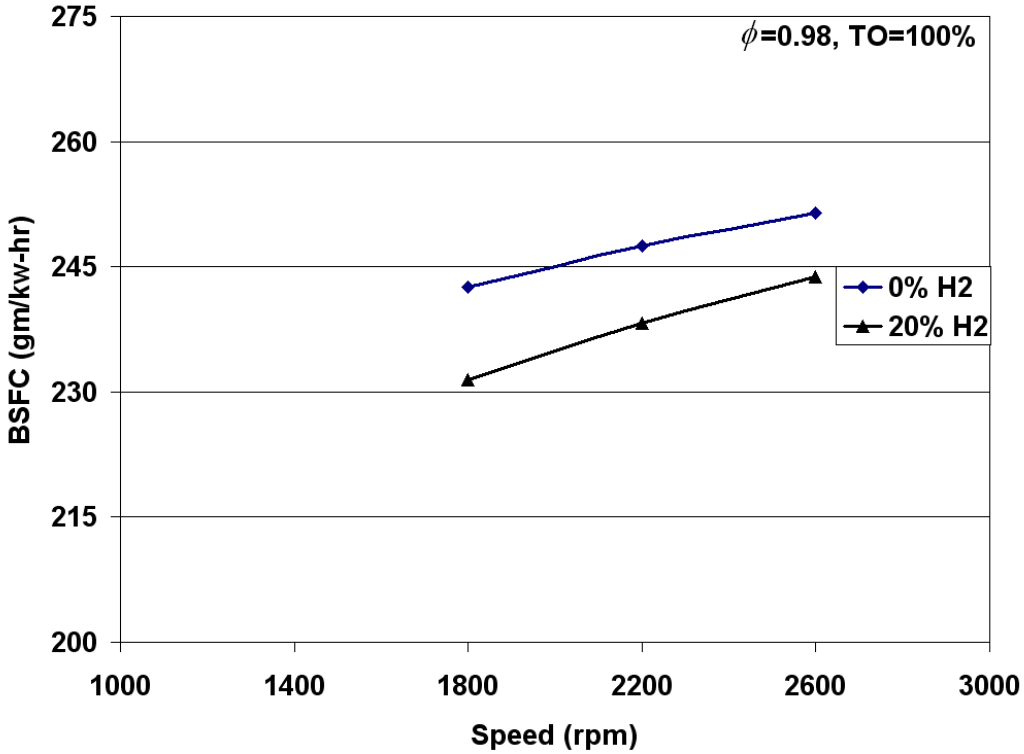

Figure 28: Variation of BSFC against speed for ϕ of 0.98 and TO of 100%

Table8: Maximum percent variation measured with 20% hydrogen for ϕ of 0.98 and TO of 100% as compared to baseline data

Description	Torque	NO_X	BTE	BSFC
Percent Change	-2	-24	+1	-5

According to Paul and James (2005) the concentration of OH and H is controlled by:

$$OH + H \leftrightarrow H_2 + O \quad (34)$$

$$OH + O \leftrightarrow O_2 + H \quad (35)$$

$$OH + H_2 \leftrightarrow H_2O + H \quad (36)$$

$$OH + OH \leftrightarrow H_2O + O \quad (37)$$

The forward and reverse reaction rates are fast for reactions shown in equations (34) through (37). Late in the expansion stroke, the rate slows and effectively freezes the [CO]/[CO_2] equilibrium. These reactions are kinetically limited by the availability of each reacting species due to the relatively fast rates of the combustion process. The ratio of [CO]/[CO_2] depends on the ratio of [H] and [OH] as given by equation (33). Thus, increasing hydrogen in the fuel increases the ratio of [H] to [OH], which in turn increases the ratio of [CO]/[CO_2].

Partial Load Results

Torque

Figures 29 and 30 show the variation of torque with respect to the engine speed at equivalence ratios of 0.9 and 1.0, respectively. At the measured speeds, the engine torque was less at 50% throttle opening than 100% throttle opening (refer to Figures 12 and 13). This reduction in torque is due to the partially closed throttle plate, which reduces the intake pressure and fuel flow rate (Heywood 1988). The plots for 50% throttle opening show a similar trend as the plots for 100% throttle opening. After conducting an uncertainty analysis, the maximum reduction in torque for all fuel blends was about 1% for an equivalence ratio of 0.9 and 2% for an equivalence ratio of 1.0 as compared with the baseline case.

CO Emissions

Figures 31 and 32 show the variation of CO emissions with respect to engine speed at equivalence ratios of 0.9 and 1.0, respectively. The measured CO emissions are higher for 50% throttle opening as compared to the tests with the throttle opened 100% (Figures 15 and 16). This can be attributed to the decrease in cylinder temperatures and pressures associated with a lower throttle opening (Bauer, 1999). After taking into consideration uncertainty, it can be concluded that at a 0.90 equivalence ratio the CO reduction between the 0% and 10% blend, and between the 10% and 20% blends was statistically significant. However, the CO measurements at 30% were statistically similar to those measured at 20%. For example, the minimal percent decrease

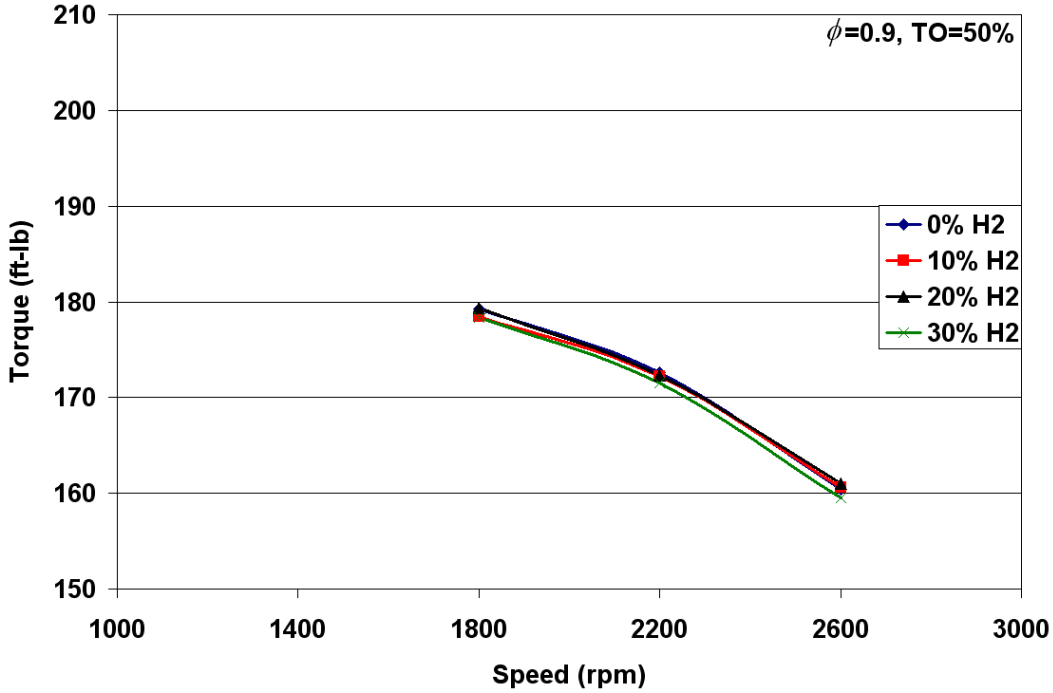

Figure 29: Variation of torque against speed for ϕ of 0.9 and TO of 50%

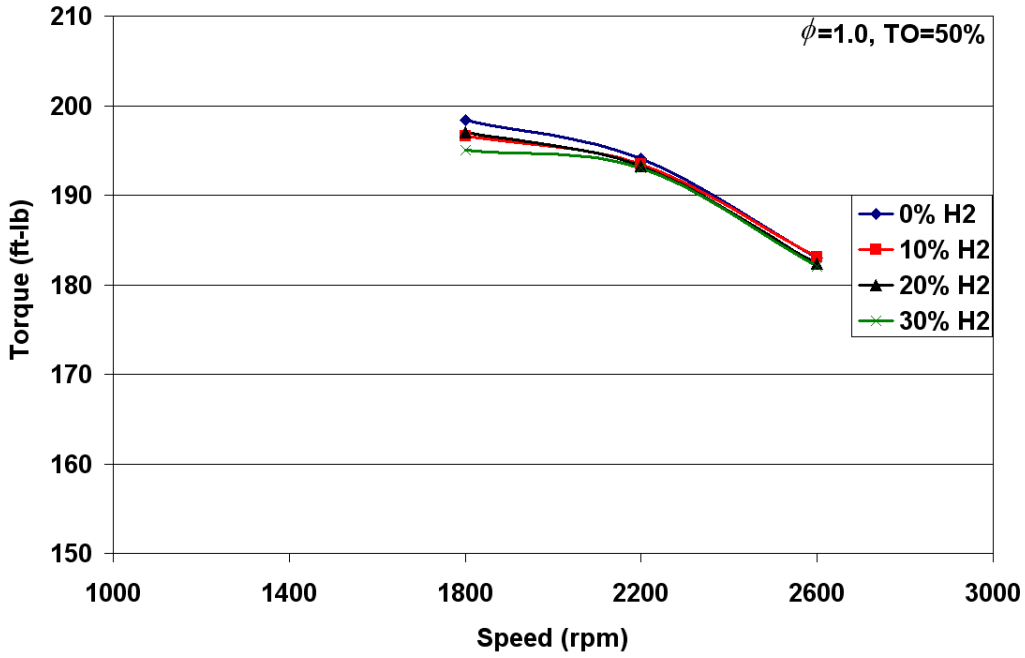

Figure 30: Variation of torque against speed for ϕ of 1.0 and TO of 50%

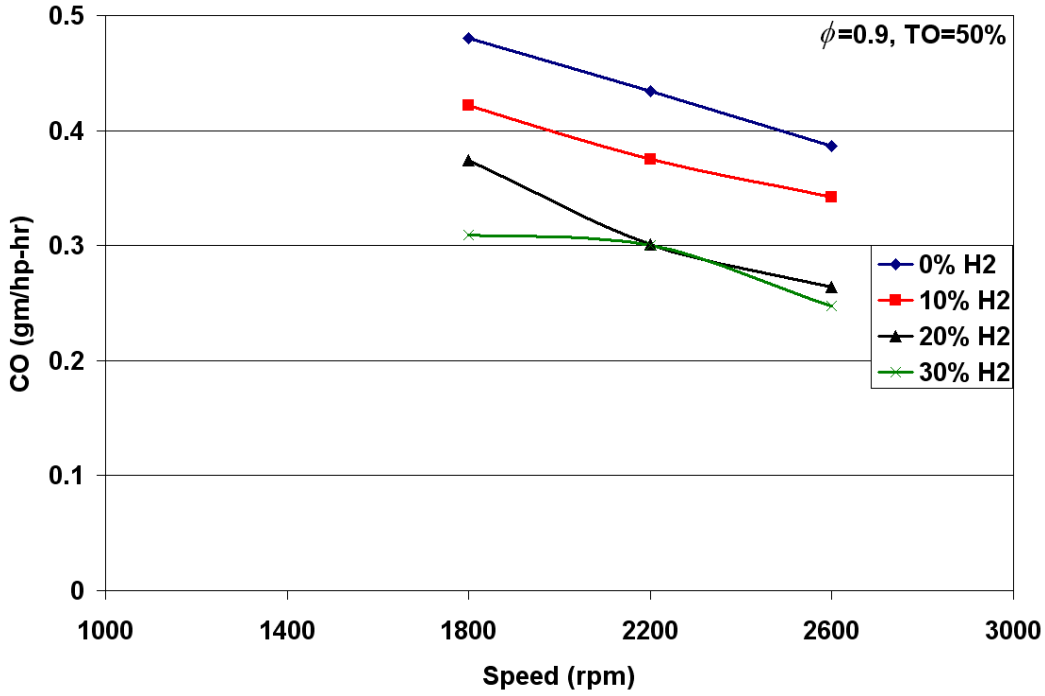

Figure 31: Variation of CO emissions against speed for ϕ of 0.9 and TO of 50%

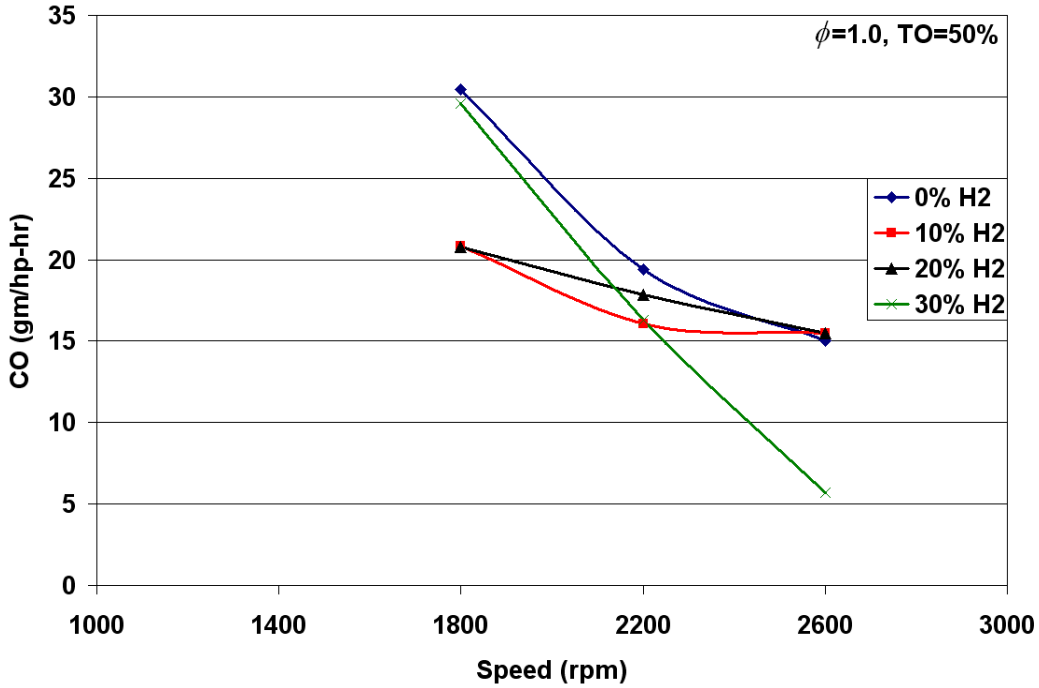

Figure 32: Variation of CO emissions against speed for ϕ of 1.0 and TO of 50%

in CO emissions between 20% and 30% hydrogen/natural blends at 2,600 rpm is about 0.13%. As explained in the full load section, an increase in percent occurs because of the increase in the combustion temperature. Furthermore, significant amounts of CO will be present due to the dissociation of CO_2 at high temperatures of about 1,800 K (Lefebvre, 1999). Though a reduction in CO emissions was measured for both the equivalence ratios (0.9 and 1.0), a good conclusion for equivalence ratio of 1.0 cannot be made because of the sensitivity associated with stoichiometric combustion. For an equivalence ratio of 0.9 and 30% hydrogen/natural gas blend, a maximum reduction of 36% in CO emissions was measured when compared with the baseline case.

These results compare favorably to those reported by Paul and James (2005), where they measured a reduction in CO emissions of about 55%.

NO_X Emissions

Figures 33 and 34 show the variation of NO_X emissions with respect to engine speed at equivalence ratios of 0.9 and 1.0, respectively. After conducting an uncertainty analysis, increasing hydrogen concentration from 20% to 30% did not reduce NO_X emissions in a statistically significant manner. The plots for 50% throttle opening (Figures 33 and 34) show similar patterns as that of 100% throttle opening (Figures 18 and 19). The percent reduction in NO_X emissions measured at 20% hydrogen with a 0.9 equivalence ratio is about 13% and about 31% for a 1.0 equivalence ratio as compared to the baseline case. Interestingly, Paul and James (2005) reported no change in NO_X emissions at part load.

Brake Thermal Efficiency (BTE)

Figures 35 and 36 show the variation of BTE emissions with respect to engine speed at equivalence ratios of 0.9 and 1.0, respectively. BTE calculated for 50% throttle opening is less than that at 100% throttle opening (Figures 20 and 21) due to the increase in the pumping loss that is associated with closing the throttle plate (Bauer, 1999). For both equivalence ratios the calculated efficiency for the measured hydrogen/natural gas blends overlaps in the uncertainty zone, which indicates no significant change in the efficiency.

Brake Specific Fuel Consumption

Figures 37 and 38 show the variation of brake specific fuel consumption with respect to engine speed at equivalence ratios of 0.9 and 1.0, respectively. As the hydrogen percentage is increased, the BSFC decreases and follows a similar trend as that for full load conditions (Figures 22 and 23).

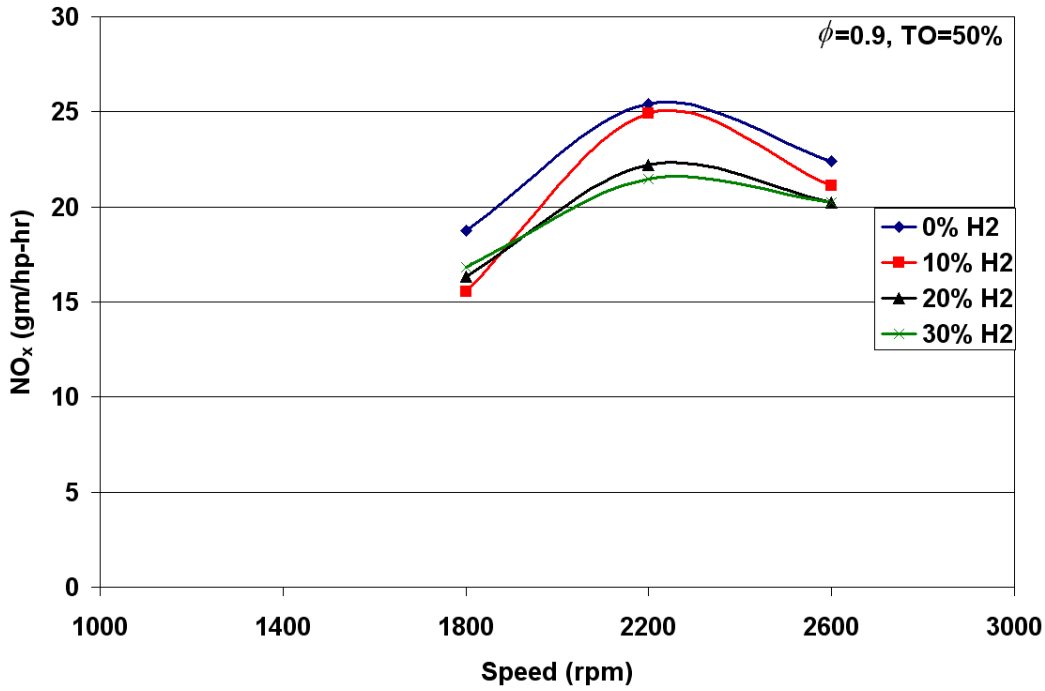

Figure 33: Variation of NO_X emissions against speed for ϕ of 0.9 and TO of 50%

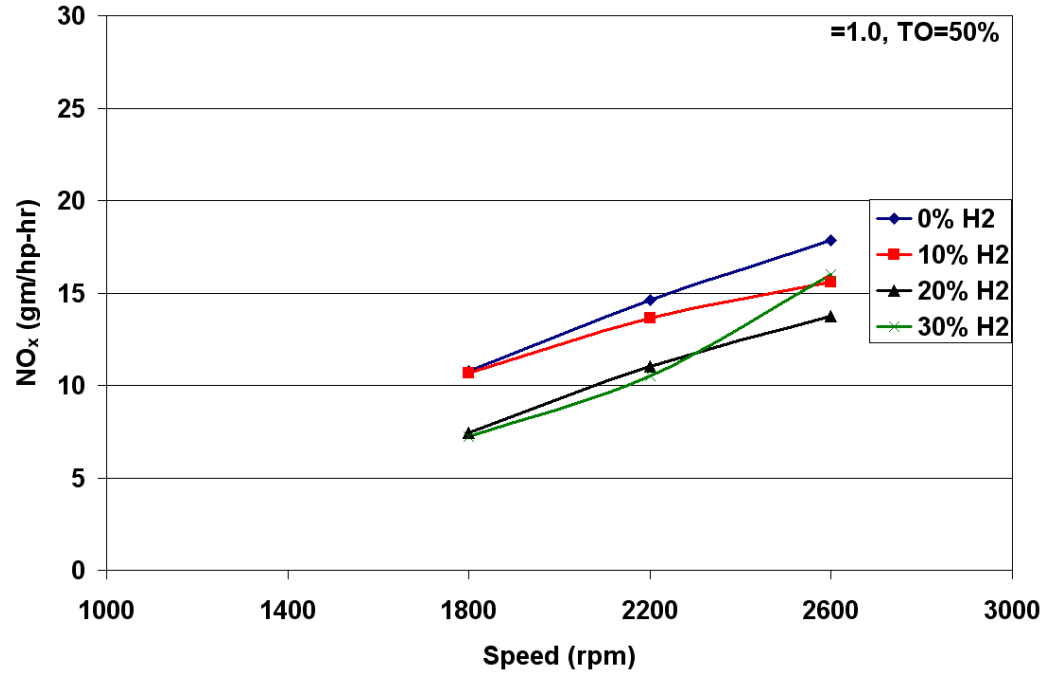

Figure 34: Variation of NO_X emissions against speed for ϕ of 1.0 and TO of 50%

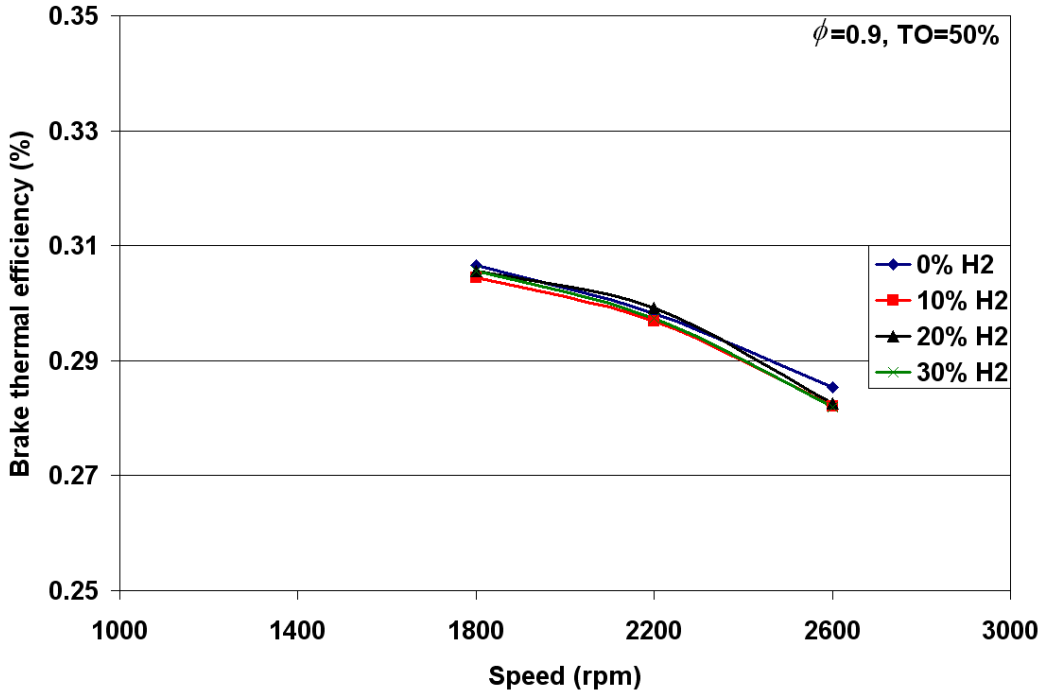

Figure 35: Variation of BTE against speed for ϕ of 0.9 and TO of 50%

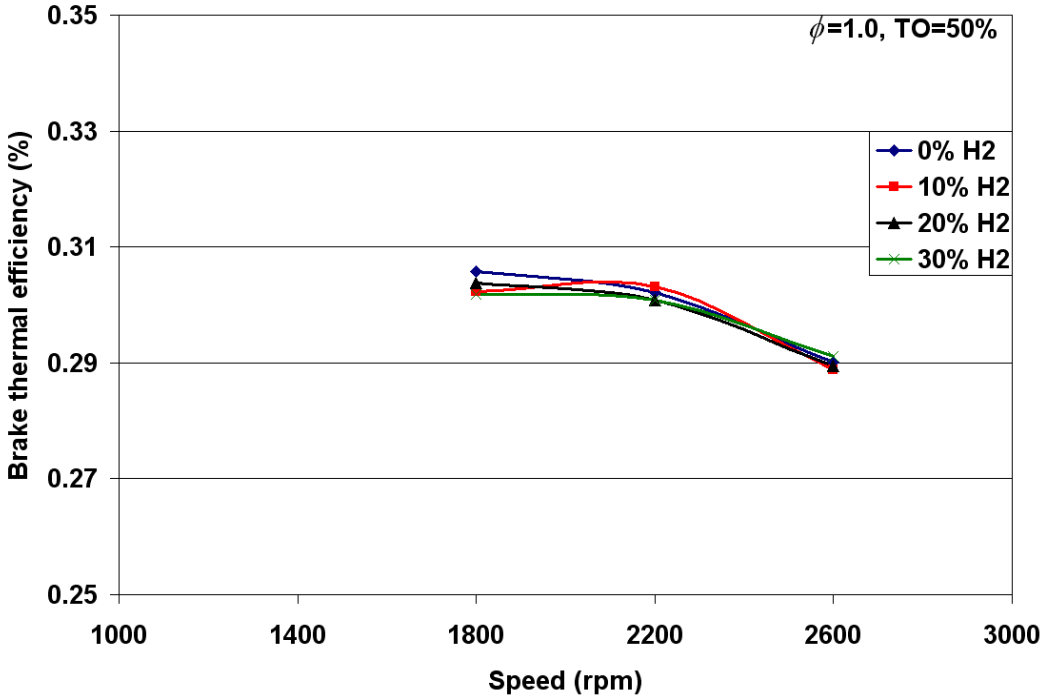

Figure 36: Variation of BTE against speed for ϕ of 1.0 and TO of 50%

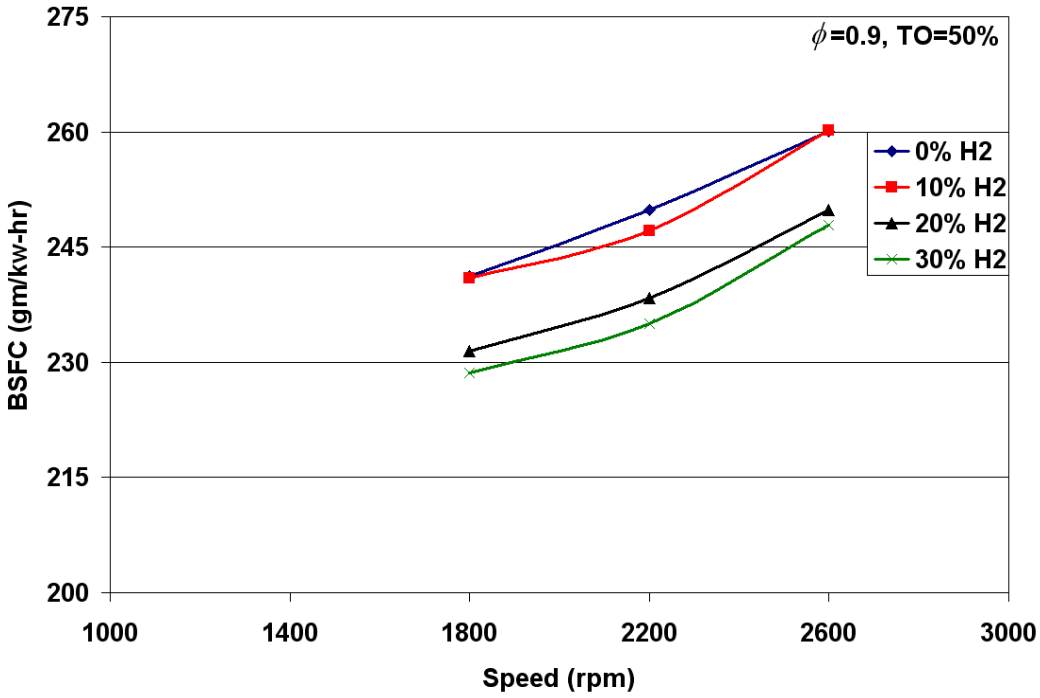

Figure 37: Variation of BSFC against speed for ϕ of 0.9 and TO of 50%

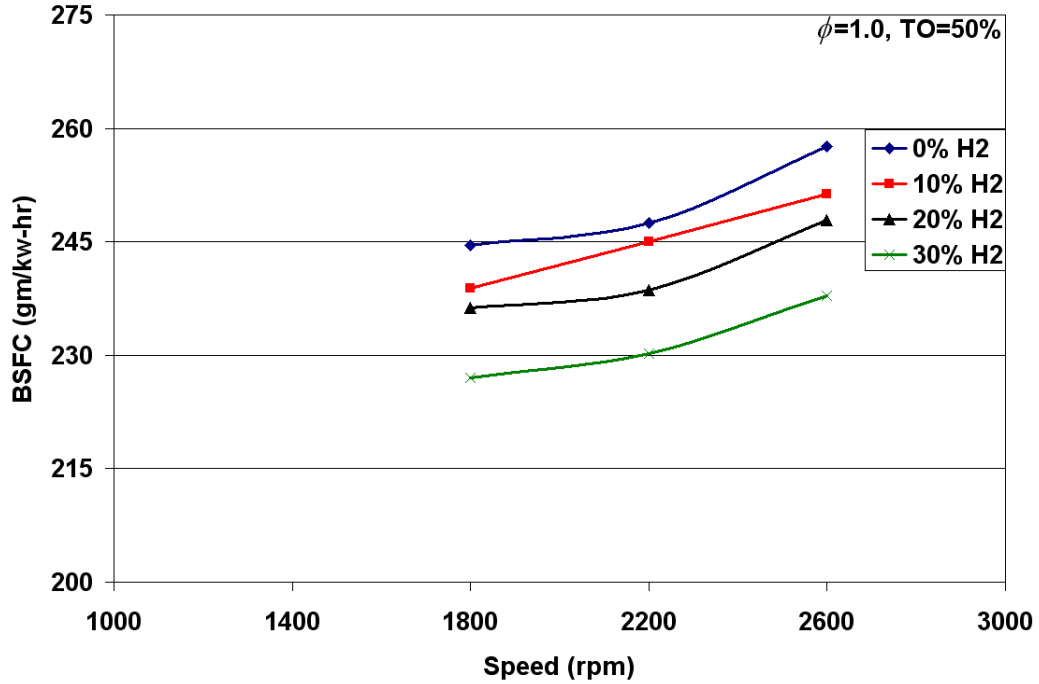

Figure 38: Variation of BSFC against speed for ϕ of 1.0 and TO of 50%

Retard Ignition Timing Results

The above plots indicated that the addition of 20% hydrogen by volume with natural gas reduces emissions with little affect on engine performance. The study was continued with this fuel blend to measure the impact when ignition timing was retarded toward top dead center (TDC). The hypothesis was that retarding the ignition timing would increase the charge temperature during flame initiation and propagation, which would then speed the reactivity of the mixture because of the high concentration of hydrogen (Attar, 1998). The shorter combustion period theoretically would decrease NO_X emissions further because NO_X formation is a function of combustion temperature and residence time.

Two sets of tests were conducted. The first, shown in Tables 9 and 11, were conducted with the ignition timing retarded 5 degrees from the baseline values shown in Figures 39 and 40. Then, the timing was altered until the difference in NO_X emissions between the two consecutive points (ignition time) did not vary in the range of 600 – 700 ppm and did not reduce the engine torque more than 5%.

Since CO emissions are very sensitive to an equivalence ratio of 1.0 (Figures 16 and 32), the ignition timing was only altered for an equivalence ratio of 0.9. Figures 39 and 40 show the change in ignition timing for a 20% hydrogen/natural gas blend with throttle openings of 50% and 100%, respectively.

Tables 9 through 12 show the percentage change with reference to base line data for torque, exhaust gas emissions (CO and NO_X), BTE and BSFC for 50% and 100% throttle openings.

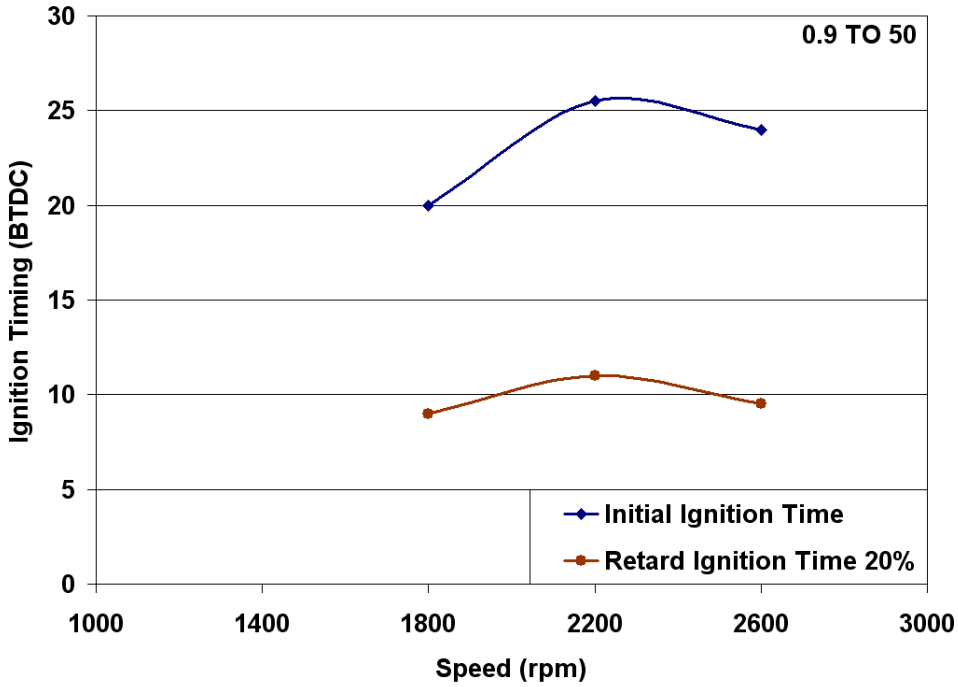

Figure 39: Spark retard for ϕ=0.9 and TO 50%

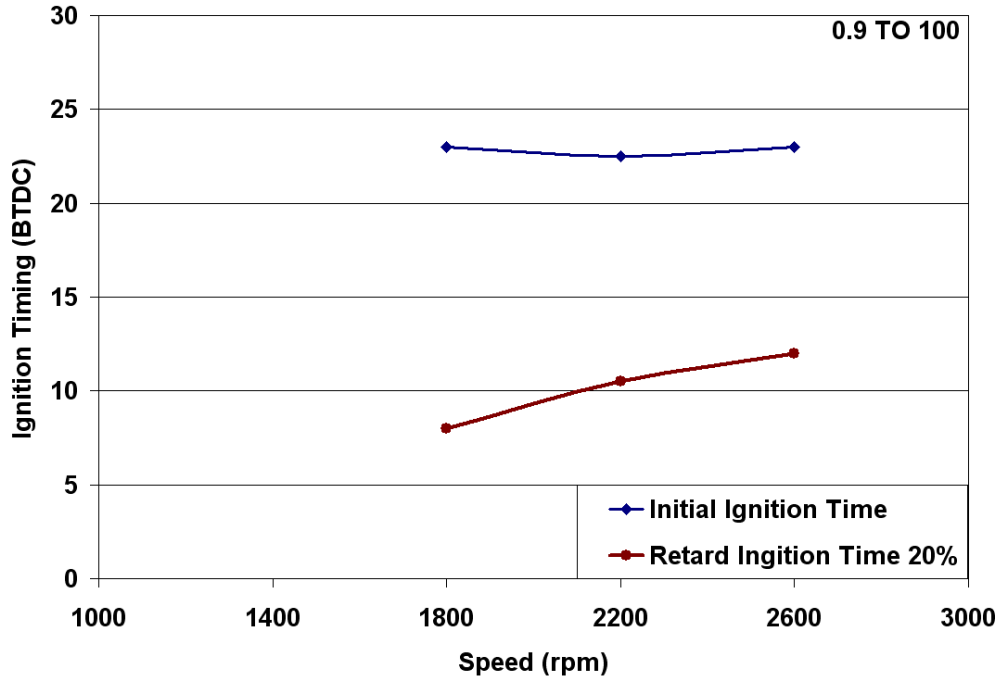

Figure 40: Spark retard for ϕ=0.9 and TO 100%

Table 9: Percentage change for ϕ of 0.9, 100% TO and MBT timing - 5° with respect to baseline

Speed (rpm)	Torque (%)	CO (%)	NO_X (%)	BTE (%)	BSFC (%)
1,800	-4	-31	-26	+4	-9
2,200	-3	-26	-38	+3	-7
2,600	-1	-28	-33	+2	-6

These data shows significant reductions in CO and NO_X, which are comparable to the results of Shudo et al. (2000). They too, observed that retarding ignition timing decreases the exhaust gas emissions without adversely affecting engine efficiency.

Table 10: Percentage change for ϕ of 0.9, 100% TO and new retard IT (refer to Figure 40) with respect to baseline

Speed (rpm)	Torque (%)	CO (%)	NO_X (%)	BTE (%)	BSFC (%)
1,800	-5	-19	-58	-1	-4
2,200	-6	-22	-61	-2	-3
2,600	-3	-17	-60	-1	-4

Table 11: Percentage change for ϕ of 0.9, 50% TO and MBT timing - 5° with respect to baseline

Speed (rpm)	Torque (%)	CO (%)	NO_X (%)	BTE (%)	BSFC (%)
1,800	-1	-31	-36	-1	-4
2,200	-0	-38	-34	0	-5
2,600	+1	-36	-31	-1	-4

Table 12: Percentage change for ϕ of 0.9, 50% TO and new retard IT with respect to baseline

Speed (rpm)	Torque (%)	CO (%)	NO_X (%)	BTE (%)	BSFC (%)
1,800	-2	-28	-49	-3	-2
2,200	-2	-21	-65	-3	-2
2,600	-4	-6	-66	-6	+1

Conclusion

The key conclusion from these tests is the modest thermal efficiency gain of about 2% and significant emission reductions of between 18% and 45% when blending hydrogen with natural gas. The optimal fuel blend was found to be 20% hydrogen with 80% natural gas. Increasing the blend to 30% hydrogen did not, in most cases, achieve a significant reduction in emissions and reduced the power produced by the engine.

Results obtained can be summarized as follows for 20% hydrogen/natural gas blends when compared to the baseline data:

1. For an equivalence ratio of 0.9 and throttle opening of 50%
    a. Maximum reduction in torque is about 1.0%
    b. Maximum reduction in emissions of CO is about 36% and NO_X is about 15%
    c. No significant change in BTE
2. For an equivalence ratio of 0.9 and throttle opening of 100%
    a. Maximum reduction in torque is 0.5%
    b. Maximum reduction in emissions of CO is about 25% and NO_X is about 18%
    c. Maximum increase in BTE is about 2.5%
5. For an equivalence ratio of 1.0 and throttle opening of 50%
    a. Maximum reduction in torque is 1%
    b. Maximum reduction in emissions of CO is about 45% and NO_X is about 31%
    c. No significant change in BTE
6. For an equivalence ratio of 1.0 and throttle opening of 100%
    a. Maximum reduction in torque is 2%
    b. Maximum reduction in emissions of CO is about 22% and NO_X is about 30%
    c. Maximum increase in BTE is about 3%

The results obtained can be compared with that of literature available in the public domain and is summarized in Figure 41.

Further reduction in emissions can be obtained by retarding the ignition timing. As CO emissions were very sensitive to the equivalence ratio close to stoichiometric conditions, ignition timing was only retarded for an equivalence ratio of 0.9. A reduction in emissions in the range of 20 – 28% for CO and 60 – 65% for NO_X can be obtained by retarding the ignition timing. However, this will reduce the engine torque by about 5%.

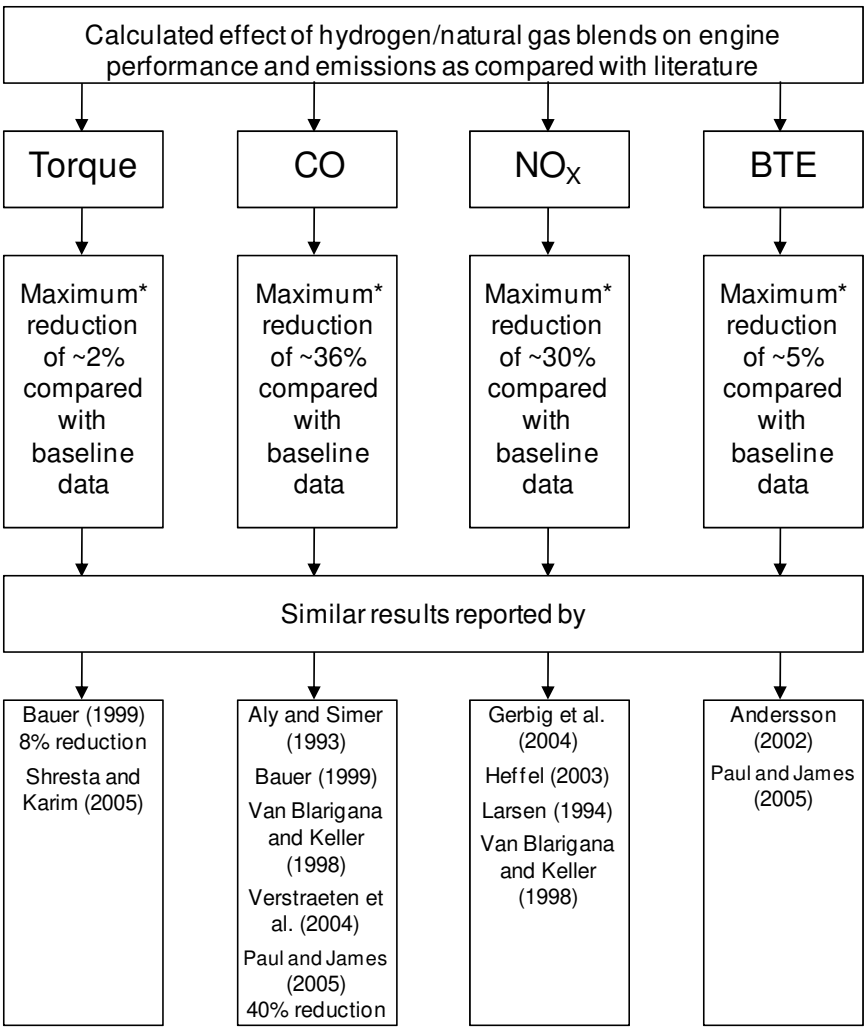

* Maximum reduction includes data collected for equivalence ratios of 0.9 and 1.0 at throttle openings of 50% and 100%.

Figure 41: Comparison of the research data with that of the literature

CO emissions decreased with a hydrogen/natural gas fuel blend because hydrogen has lower carbon content than natural gas. The literature shows NO_X emission reductions with hydrogen/natural gas fuel blends may be due one of the following reasons: shorter combustion duration, higher diffusivity of hydrogen and increased residual gas. Also, the brake thermal efficiency for most data points improved because of the advantages associated with hydrogen addition such as an increase in the burn rate and the specific heat ratio, and improved combustion efficiency.

Hydrogen addition to natural gas seems to be a viable solution to reduce emissions without a significant loss in engine efficiency and power output. Also hydrogen/natural gas blends can act as a transition fuel to the use of only hydrogen as a fuel. Issues associated with hydrogen use such as backfire, safety, hydrogen production and transportation costs have to be overcome.

Graphical Materials Lists

References

Alcock, J. L., 2001, "Complication of Existing Safety Data on Hydrogen and Comparative Fuels," EIHP2, Contract ENK6-CT2000-00442.

Aly, H., and Siemer, G., 1993, "Experimental Investigation of Gaseous Hydrogen Utilization in a Dual-Fuel Engine for Stationary Powerplants," ASME, Internal Combustion Engine Division, Alternate Fuels, Engine Performance and Emission, ICE Vol. 20, pp. 67-79.

American Meteorological Society, 2000, "Clean Air Act of 1990." Legislation: A look at US Air pollution Laws and their Amendments.

Andersson, T., 2002, "Hydrogen Addition for Improved Lean Burn Capability on Natural Gas Engine," Report SGC 134, Lund Institute of Technology.

Attar, A.A., 1998, "Knock Rating of Gaseous Fuels," ASME Fall Conference, Vol. 31, pp. 41-47.

Azar, C., Kristain L., and Bjorn A., 2003, "Global Energy Scenarios Meeting Stringent CO2 Constraints – Cost Effective Fuel Choices in the Transportation Sectors," *Energy Policy*, Vol. 31, pp. 961-976.

Bauer, C., 1999, "The Effect of Hydrogen on the Performance of Methane-fuelled S.I Engines," Thesis, University of Alberta.

Bauer, C.G., and Forest, T.W., 1999, "Effect of Hydrogen Addition on the Performance of Methane-Fueled Vehicles. Part I: Effect on S.I. Engine Performance," *International Journal of Hydrogen Energy*, Vol. 26, No. 1, pp. 55-70.

Bevington, P.R, and Robinson, D.K., 2003, *Data Reduction and Error Analysis for the Physical Sciences, Third Ed.*, McGraw-Hill, Boston, Massachusetts..

Campbell, C.J., 2002, *Hubbert Center Newsletter, 2002-03*, "Forecasting Global Oil Supply 2000-2050", Colorado School of Mines.

Caris, D. F., and Nelson, E. E., 1959, "A New Look at High Compression Engines," *SAE Transactions*, Vol. 67, pp. 112-124.

Cengel, Y., and Boles, M., 2002, *Thermodynamics an Engineering Approach*, McGraw-Hill, Inc., New York.

Das, L.M., 1996, "Hydrogen-Oxygen Reaction Mechanism and its Implication to Hydrogen Engine Combustion," *International Journal Hydrogen Energy*, Vol. 21, pp. 703-715.

Das, L. M., 1990, "Hydrogen Engines: A View of the Past and a Look into the Future," *International Journal of Hydrogen*, Vol. 15 pp. 425-443.

Edison, M. H., and Taylor, C. F., 1964, "The Limits of Engine Performance – Comparison of Actual and Theoretical Cycles," Digital Calculations of Engine Cycles, SAE Prog. in Technology, Vol.7, pp. 65-81.

Ely, C., 2004, "Emission Data Collection, Calculation, and Interpretation," Engine Emissions Stack Testing & Analyzer Workshop, Oklahoma City, Oklahoma.

Energy Information Administration, 2007, International Energy Outlook 2007, DOE/EIA-0484.

Ferguson, C. R., and A. R. Kirkpatrick, 2000, *Internal Combustion Engines*, New York, NY: John Wiley & Sons.

GAO., 2007, "Crude Oil: Uncertainty about Future Oil Supply Makes it Important to Develop a Strategy for Addressing a Peak and Decline in Oil Production," Report to Congressional Requesters, GAO-07-283.

Gerbig, F., Strobl, W., Eishlseder, H., and Wimmer, A., 2004, "Potentials of the Hydrogen Combustion Engine with Innovative Hydrogen-Specific Combustion Process," Institute of Internal Combustion Engines and Thermodynamics, Austria.

Heffel, J. A., 2003, "NO_X Emission and Performance Data for a Hydrogen Fueled Internal Combustion Engine at 1500 rpm using Exhaust Gas Recirculation," *International Journal of Hydrogen Energy*, Vol. 28, pp. 901-08.

Heywood, J.B., 1988, *Internal Combustion Engine Fundamentals*, New York, McGraw Hill.

International Organization of Standards, ISO 5167-2, 2003, Measurement of Fluid Flow by Means of Pressure Differential Devices Inserted in Circular Cross-section Conduits Running Full – Part 2: Orifice Plates.

Karim, G. A., Wierzba, I., and Al-Alousi, Y., 1996, "Methane-Hydrogen Mixtures as Fuels," *International Journal of Hydrogen Energy*, Vol. 21, No. 7, pp. 625-631.

Kenneth, K.K., 2005, *Principles of Combustion, 2nd Ed.*, John Wiley & Sons, New Jersey.

Lefebvre, A.H., 1999, *Gas Turbine Combustion, 2nd Ed.*, Taylor & Francis, Philadelphia, Pennsylvania.

Nagalingam, A., Duebel, F., and Schmillen, K., 1983**,** "Performance Study Using Natural Gas, Hydrogen-Supplemented Natural Gas and Hydrogen in AVL Research Engine," *International Journal of Hydrogen Energy*, Vol. 8, pp. 715-720.

Paul, A.S., and James, S.W., 2005, "Effect of Hydrogen Content in Hydrogen Natural-Gas Fuel Mixtures on Emissions in a Lean-Burn IC Engine," ASME 2005 Fall Conference, pp. 363-371.

Polasek, M., Macek, J., and Takats, M., 2002, "Hydrogen Fuelled Engine – Properties of Working Cycle and Emission Potentials," FISITA World Automotive Congress, Helsinki, Finland.

Pulkrabek., W.W., 1997, *Engineering Fundamentals of the Internal Combustion Engine*, Prentice Hall, Upper Saddle River, New Jersey.

Ryan, T. W., 2003, "Diesel Engine Alternatives," Diesel Engine Conference Emissions Reduction.

Shreshta B.S.O., and Karim, G.A., 2005, "The Operational Mixture Limits in Engines Fueled with Alternative Gaseous Fuels," ASME Spring Conference, pp. 319-325.

Shrestha, B.S.O., Karim, G.A., 1999, "Hydrogen as an Additive to Methane for Spark Ignition Engine Applications," *International Journal of Hydrogen Energy*, Vol. 24, No. 6, pp. 577-586.

Shudo, T., Shimamura, K., and Nakajima, Y., 2000**,** "Combustion and Emissions in a DI Stratified Charge Engine with Hydrogen Pre-Mixing," *JSAE Review*, Vol. 21, pp. 3-7.

Sierens, R., and Verhelst, S., 2001, "Hydrogen Engine Specific Properties," *International Journal of Hydrogen*, Vol. 26, pp. 987-990.

Skrebowski., C., 2004, "Oil Field Mega Projects 2004," Petroleum Review January 2004.

TSI Incorporated, 2004, Series 6300 CA-Calc ™ Compliance Protocol Emissions Analyzers: Operation and Service Manual, 198050, Revision A, Shoreview, Minnesota.

Van Blarigan, P., and Keller, J.O., 1998, "A Hydrogen Fueled Internal Combustion Engine designed for Single Speed/Power Operation," *International Journal of Hydrogen Energy*, Vol. 23, pp.603-609.

Verstraeten, S., Verhelst, S., and Sierens, R., 2004, "Development of A Single Cylinder IC Engine for Hydrogen," 10th International Congress CONAT 2004, Brasov, Romania.

Xavier, F-A., 2000, "Uncertainty of Measurement in Clinical Laboratory Sciences," *Clinical Chemistry*, Vol. 46 No. 9, pp. 1437-38.

List of Acronyms

AFR	Air-to-fuel ratio
BSFC	Brake specific fuel consumption
BTE	Brake thermal efficiency
bhp	Brake horsepower
Btu	British thermal unit
cc	Cubic centimeters
CID	Cubic inch displacement
CNG	Compressed natural gas
CO	Carbon monoxide
CO_2	Carbon dioxide
CTM	Conditional Test Method
DC	Direct current
DOE	Department of Energy
EGR	Exhaust gas recirculation
ER	Equivalence ratio
EPA	Environmental Protection Agency
EPM	Engine performance module
EPR	Electronic pressure regulator
F	Degree Fahrenheit
FS	Full scale
Ft-lbm	Foot-pound mass
G	Grams
g/bhp-hr	Grams per brake horsepower-hour
g/kW-hr	Grams per kilowatt-hour
H	Hydrogen
HC	Hydrocarbons
hp	Horsepower
in	Inches

In-HgA	Inches of mercury absolute
IC	Internal combustion
ICE	Internal combustion engine
in-WC	Inches of water column
I/O	Input output
IT	Ignition timing
K	Kelvin
kPA	Kilo Pascal
kg	Kilograms
kgf	Kilograms force
kg/m^3	Kilograms per cubic meter
kg.sec	Kilograms per second
kJ/mol	Kilojoules per mole
KW	Kilowatts
lb	Pounds
lbf	Pounds force
lbm	pounds mass
LFE	Laminar flow element
m	Meter
mA	Miliamperes
MBT	Maximum brake torque
min	Minute
mm	milimeters
mJ	Millijoule
mJ/kg	Millijoule per kilogram
MMBtu	Million British thermal units
m/s	Meters per second
mtoe	Million tonne oil equivalent
mV	See table 3: torque measurement and sensors
N	Nitrogen
Nm	Newton meters

NMHC	Non-methane hydrocarbons
NO	Nitrogen oxide
NO_2	Nitrogen dioxide
NO_X	Oxides of nitrogen
O_2	Oxygen
OEM	Original equipment manufacturer
OH	Hydroxyl
ppm	Parts per million
ppmv	Parts per million by volume see page 26
psia	Pounds per square inch absolute
psig	Pounds per square inch gage
pt	Point
R	Degree Rankine
rpm	Revolutions per minute
SCF	Standard cubic feet
sec	Second
TO	Throttle open
TDC	Top dead center
vol	Volume
WOT	Wide open throttle

Nomenclature

A	Area
AFR	Air-to-fuel ratio
B	Flow meter constant
C	Flow coefficient
C_f	Correction factor
c	Specific heat
d	Dry
E	Activation energy, emissions
e	Gas expansibility factor
F_{Btu}	Emissions factor
K	Chemical equilibrium constant
k	Ratio of constant pressure and constant volume specific heats; kinetic coefficients
LHV	Lower heating value
M	Molecular weight
m	Mass
$\dot{m}$	Mass flow rate
N	Rotating speed or number of moles
n	Moles per mole of fuel
p	Pressure
P_R	Pressure ratio
Q	Heat transfer

$\dot{Q}$	Rate of heat transfer
q	Specific heat transfer
$\dot{q}$	Specific rate of heat transfer
R	Gas specific gas constant, R_u / M
r	Radius
R_u	Universal gas constant
T	Temperature
t	Time
v	Specific volume
$\dot{V}$	Volumetric flow rate
Y	Specific volume
W	Work
$\dot{W}$	Power
w	Specific work
$\dot{w}$	Specific rate of doing work (specific power)
y	Mole fraction
Z	Compressibility factor

Greek Variables

α	Number of carbon atoms
β	Beta ratio; number of hydrogen atoms
Δ	Change in a condition, as in Δp is the change in pressure
μ	Viscosity
η_b	Brake thermal efficiency
η_v	Volumetric efficiency

ρ	Density
τ	Torque
ϕ	Air-fuel based equivalence ratio [AFR_{stoich}/AFR]

Subscripts

a	Air
act	Actual
b	Brake quantity
cr	Critical thermodynamic condition
d	Dry
e	See eq 17
F	Fuel; friction
f	Fuel
i	Species with a mixture; indicated quantity
in	Inlet
m	Measured
Mass	Mass
mix	Mixture of gas
ppmv	Parts per million by volume
R	Reactants; reduced quantity
r	Reference condition
std	Standard air
stoich	Stoichiometric
th	Throat of orifice plate
v	Vapor
V	Vapor

Appendix A: Calculation for Combustion Chamber Occupied by Hydrogen

The stoichiometric combustion of hydrogen and air is given as:

$$2H_2 + O_2 \rightarrow 2H_2O \tag{A.1}$$

Moles of H_2 for complete combustion = 2 moles

Moles of O_2 for complete combustion = 1 mole

Moles of N_2 in air:

$$= \text{Moles of } O_2 \times \left[\frac{79\%\ N_2 \text{ in air}}{21\%\ O_2 \text{ in air}}\right]$$

$$= 1 \text{ mole of } O_2 \times \left[\frac{79\%\ N_2 \text{ in air}}{21\%\ O_2 \text{ in air}}\right]$$

$$= 3.762 \text{ moles } N_2$$

Number of moles of air:

$$= \text{Moles of } O_2 + \text{moles of } N_2$$

$$= 1 + 3.762$$

$$= 4.762 \text{ moles of air}$$

Weight of O_2:

$$= 1 \text{ mole of } O_2 \times 32 \text{ g/mole}$$

$$= 32 \text{ g}$$

Weight of N_2:

$$= 3.762 \text{ moles of } N_2 \times 28 \text{ g/mole}$$

$$= 105.33 \text{ g}$$

Weight of air:

$$= \text{Weight of } O_2 + \text{weight of } N_2 \tag{A.2}$$

$$= 32 \text{ g} + 105.33 \text{ g}$$

$$= 137.33 \text{ g}$$

Weight of H_2:

$$= 2 \text{ moles of } H_2 \times 2 \text{ g/mole}$$
$$= 4 \text{ g}$$

Stoichiometric air/fuel ratio for hydrogen and air is:

$$= \frac{\text{mass of air}}{\text{mass of fuel}}$$
$$= \frac{137.33 \text{ g}}{4 \text{ g}}$$
$$= 34.33 : 1$$

Air-to-fuel ratio based on volume:

$$= \frac{\text{Volume (moles) of air}}{\text{Volume (moles) of fuel}}$$
$$= \frac{4.762}{2}$$
$$= 2.4 : 1$$

The percent of the combustion chamber occupied by hydrogen for a stoichiometric mixture:

$$= \frac{\text{Volume (moles) of } H_2}{\text{Total volume}}$$
$$= \frac{\text{Volume of } H_2}{\text{Volume of air+Volume of } H_2}$$
$$= \frac{2}{4.762 + 2}$$
$$= 29.6\%$$

Similarly, it can be shown that the percent of the combustion chamber occupied by methane for a stoichiometric mixture is 9.5675.

Appendix B: Uncertainty Calculation

The following is an example on how the uncertainty analysis is calculated:

$$E_{\mathrm{CO}} = \left[y_i \times n_R \times M_i\right]\left[\frac{1000[\mathrm{gm}]}{\mathrm{kg}} \times \frac{3600[\mathrm{sec}]}{\mathrm{hr}}\right]\left[\frac{1}{10^6 \times \dot{W}_{act}}\right]\left[\frac{\dot{m}_f[\mathrm{kg/sec}]}{M_f}\right]$$

Given:

$$n_R = 8.995$$
$$M_i = 14$$
$$M_f = 28$$
$$W_{act} = 69.5354$$
$$m_f = 0.00340783$$
$$y_i = 126$$
$$dy_i = 12.6$$
$$dm_f = 2.687 \times 10^{-5}$$
$$dW = 0.152$$

Then:

$$dE = \frac{n_R \times M_i \times 1000 \times 3600}{10^6 \times M_f}\sqrt{\left(\frac{\mathrm{dy_i} \times \dot{m}_f}{\dot{W}_{act}}\right)^2 + \left(\frac{\mathrm{y_i} \times d\dot{m}_f}{\dot{W}_{act}}\right)^2 + \left(\frac{\mathrm{y_i} \times \dot{m}_f \times dW}{-\dot{W}_{act}^2}\right)^2}$$

$$dE = 0.01$$